JOURNAL OF VIROLOGY, Apr. 2005, p. 3903–3919 Vol. 79, No. 7
0022-538X/05/$08.00+0 doi:10.1128/JVI.79.7.3903–3919.2005

Heterogeneity of a Fluorescent Tegument Component in Single Pseudorabies Virus Virions and Enveloped Axonal Assemblies

T. del Rio,[1]†‡ T. H. Ch'ng,[1]† E. A. Flood,[1] S. P. Gross,[2] and L. W. Enquist[1]*

Department of Molecular Biology, Princeton University, Princeton, New Jersey,[1] and Department of Developmental and Cell Biology, University of California, Irvine, California[2]

Received 14 September 2004/Accepted 13 January 2005

The molecular mechanisms responsible for long-distance, directional spread of alphaherpesvirus infections via axons of infected neurons are poorly understood. We describe the use of red and green fluorescent protein (GFP) fusions to capsid and tegument components, respectively, to visualize purified, single extracellular virions and axonal assemblies after pseudorabies virus (PRV) infection of cultured neurons. We observed heterogeneity in GFP fluorescence when GFP was fused to the tegument component VP22 in both single extracellular virions and discrete puncta in infected axons. This heterogeneity was observed in the presence or absence of a capsid structure detected by a fusion of monomeric red fluorescent protein to VP26. The similarity of the heterogeneous distribution of these fluorescent protein fusions in both purified virions and in axons suggested that tegument-capsid assembly and axonal targeting of viral components are linked. One possibility was that the assembly of extracellular and axonal particles containing the dually fluorescent fusion proteins occurred by the same process in the cell body. We tested this hypothesis by treating infected cultured neurons with brefeldin A, a potent inhibitor of herpesvirus maturation and secretion. Brefeldin A treatment disrupted the neuronal secretory pathway, affected fluorescent capsid and tegument transport in the cell body, and blocked subsequent entry into axons of capsid and tegument proteins. Electron microscopy demonstrated that in the absence of brefeldin A treatment, enveloped capsids entered axons, but in the presence of the inhibitor, unenveloped capsids accumulated in the cell body. These results support an assembly process in which PRV capsids acquire a membrane in the cell body prior to axonal entry and subsequent transport.

A remarkable property of the alphaherpesvirus life cycle in the natural host is invasion and controlled spread within the peripheral nervous system (PNS) with exceedingly rare incursions into the central nervous system. The basic unit of a herpesvirus infection is the extracellular virion, a complex particle comprising several thousand protein molecules (31). Herpes virions, in general, are approximately 200 nm in diameter with a membrane envelope containing more than 12 virus-borne membrane proteins. This host-derived membrane surrounds a tegument layer of at least 12 soluble proteins, which, in turn, surrounds an icosahedral capsid containing the 142-kb genome (36, 59). The assembly and movement of these distinct virion structures must be understood at the cellular level as these properties directly influence herpesvirus pathogenesis and transmission. Pseudorabies virus (PRV), an animal pathogen, has served as a model for study of directional spread of the neurotropic herpesviruses, which include the human pathogens herpes simplex virus (HSV) and varicella-zoster virus (VZV). After replication of PRV at exposed mucosal surfaces, virion components enter the axon terminals of PNS neurons, and unenveloped capsids move toward the cell body to deliver the genome to nuclei within ganglia. In natural hosts, a latent infection is typically established in these PNS neurons. Upon reactivation, capsids are assembled in the nuclei of PNS neurons, enter axons, and are moved in an anterograde direction toward axon terminals near the site of the original infection. Such directional intracellular movement is dependent upon intact microtubules (41, 53, 64, 70) and involves transport of virion components many millions of virion diameters to and from the cell body of a neuron. Directional transport within axons is likely to be regulated by different interactions of viral proteins with cellular transport machinery during retrograde and anterograde movement on microtubules. Indeed, the differential modulation of plus- and minus-end motor-based movement of capsids early and late in infection appears to affect gross directional movement in neurons (63).

A recent model of herpesvirus assembly proposes that newly formed capsid proteins enter axons and are transported separately from membrane proteins as subassemblies of mature virions (53, 56, 69). Genetic evidence supporting this subassembly transport model derives from studies on attenuated PRV strains utilized for tracing neural circuitry. We have reported that certain viral membrane proteins control the direction of spread between neurons within a neural circuit. For example, deletion of any one of three genes, encoding glycoprotein E (gE), gI, or Us9, from the PRV genome blocks neuronal circuit spread in the anterograde direction, from an infected presynaptic neuron to the synaptically connected postsynaptic neuron (reviewed in reference 24). These gene products are not required for entry of PRV virions at axon terminals or spread in circuitry in the retrograde direction, from a postsynaptic to presynaptic neuron. Subsequent analysis has demonstrated that the Us9 protein is necessary for localization of newly synthesized viral glycoproteins into the

* Corresponding author. Mailing address: Schultz Laboratory, Department of Molecular Biology, Princeton University, Princeton, NJ 08544-1014. Phone: (609) 258-2664. Fax: (609) 258-1035. E-mail: Lenquist@molbio.princeton.edu.

† T.D.R. and T.H.C. contributed equally to this work.

‡ Present address: Neurobiology Section, Division of Biological Sciences, University of California, San Diego, La Jolla, Calif.

axonal compartment of cultured neurons but not for that of capsid or tegument proteins (69). In contrast, expression of the gE protein is required for efficient viral glycoprotein, capsid, and tegument localization to the axon but not for a subset of nonglycosylated viral membrane proteins (T. H. Ch'ng and L. W. Enquist, unpublished data). While these discoveries have identified some key viral components of directional spread, the mechanisms of viral protein-dependent axonal sorting remain to be elucidated.

How distinct virion components are coupled to motors, directly or via adaptors, is an important area of focus in the study of directional spread. Previous work has suggested two distinct alternatives. One possibility is that the viral tegument layer, the poorly understood proteinaceous layer surrounding the capsid, provides the physical connection between the capsid and different classes of motors. In this case, the tegument layer is the central component of directional movement. Upon entry at nerve terminals, the tegument-capsid structure is separated from the envelope. Some tegument proteins may dissociate from the capsid, which is moved from the plus end to the minus end of a microtubule, toward the nucleus in the retrograde direction. Following replication, the newly formed capsid and tegument layer are released into the cytoplasm and enter axons where this unique tegument layer, different from that present during entry, presumably binds kinesin motors for movement toward the plus end of a microtubule in the anterograde direction. Support for this proposal comes from studies on HSV type 1 (HSV-1) demonstrating that nonenveloped capsids are found in the axon following virus replication (33, 34, 55, 56), tegument structures form in the cell body of infected neurons (54), and the tegument protein Us11 interacts with the kinesin heavy chain (20). However, the Us11 gene is not present in many alphaherpesvirus genomes, including those of PRV and VZV (36, 52). In the absence of Us11 protein, other PRV and VZV tegument proteins must interact with motors for kinesin-mediated transport in this model. An alternative idea is that while tegument-capsid complexes are moved to the cell body following entry at axon terminals, newly replicated tegument-capsid structures are directed in the cytoplasm to axon-sorting compartments, where they acquire a cellular membrane. The absence of this membrane during capsid entry and its presence during egress provide the preferential interaction with different classes of motors. Indeed, enveloped capsids have been visualized in axons following virus replication (11, 15, 26, 40, 43, 49, 50, 75), and the tegument proteins VP22 and UL11 have been shown to associate with cellular membranes (1, 7, 38).

We used two approaches to discern the subvirion structures transported in axons following virus replication and distinguish between the unenveloped versus enveloped capsid models of axonal egress. In the first approach, we constructed PRV strains expressing two fluorescent fusion proteins: the monomeric red fluorescent protein (mRFP) fused to VP26 and the green fluorescent protein (GFP) fused to VP22. The mRFP fusion protein incorporates into capsids, while the GFP fusion protein assembles in the tegument layer. Infection by the dually fluorescent virus enabled live-cell imaging and localization of subvirion structures during virus egress. Live-cell imaging of single fluorescent virion structures, including fusion proteins similar to the ones described here, have been previously reported (4, 18, 21, 22, 23, 42, 62, 65, 73). Furthermore, dually fluorescent virus fusions have also been previously reported for HSV and have been utilized for the localization of structural proteins in the compartments of infected cells (25, 35). However, the high nucleotide sequence similarity of GFP variants can result in recombination and the exchange of fluorescence properties following cotransfection of epithelial cells (5). We avoided this complication during infection by using a monomeric red fluorescent protein with limited homology to GFP (5, 9). A recombinant PRV strain containing the mRFP marker for tracing studies has been reported previously (2), and mRFP was more suitable for the detection of virus spread than other red fluorescent proteins, such as DsRed.

The second approach used the dually fluorescent virus to investigate the connection between the reenvelopment pathway for alphaherpesvirus assembly and the entry and transport of virion subassemblies in axons. Specifically, we focused on the formation of tegument-capsid structures in the cytoplasm and their direction to the axonal compartment. Treatment of alphaherpesvirus-infected cells with brefeldin A (BFA) inhibits virus maturation and egress by disrupting transport within the secretory pathway (12, 13, 28, 39, 46, 47, 66, 72). More recently, release of a synchronous infection revealed that the primary block to HSV-1 assembly by BFA occurred prior to budding at the nuclear membrane (16). Long-term BFA application (over several hours) has been used to study the compartmentalization of virion components in infected neurons. Two key studies suggest that long-term BFA treatment of rat dorsal root ganglion neurons infected with HSV-1 blocks axonal entry of viral glycoproteins and a fraction of tegument proteins but does not block capsid entry (53, 54). In the present study, we used long-term BFA treatment to assess the effect of secretory pathway disruption on axonal entry of fluorescent capsid and tegument fusion proteins during PRV infection. Unexpectedly, BFA treatment sufficient to block viral glycoprotein axonal entry also efficiently blocked axonal entry of fluorescent fusions to capsid (mRFP-VP26) and tegument (GFP-VP22) proteins. BFA disruption of the secretory system was reversible, enabling restoration of virus assembly transport. The data presented in this study provide a new interpretation of axonal sorting, entry, and transport of alphaherpesvirus assemblies in neurons.

MATERIALS AND METHODS

Cells and virus strains. The PK15 (pig kidney) cell line was used for propagation of all PRV strains. Cells were grown in Dulbecco's modified Eagle's medium supplemented with 10% fetal bovine serum, while viral infections were performed in Dulbecco's modified Eagle's medium supplemented with 2% fetal bovine serum. Primary sympathetic neurons from the superior cervical ganglia (SCG) of rat embryos (15 to 16 days of gestation) were dissociated according to the methods of DiCicco-Bloom et al. (19, 69). The rat PC12 (pheochromocytoma) cell line was differentiated to sympathetic-type cultures with nerve growth factor (NGF) (29) in differentiation medium (14). PC12 cells were exposed to NGF for 10 days prior to freezing and storage in a primed, differentiated state (14, 30). SCG and primed PC12 cells were cultured on Delta T dishes (Bioptechs, Inc.) coated with a combination of poly-DL-ornithine and laminin as previously described (14) for 7 to 10 days and 2 days, respectively, prior to infection and imaging (see below).

Antisera. Rabbit polyclonal antiserum to VP22 (PAS 236) was raised against FL-VP22 (described below) expressed in a baculovirus system. Sf9 cells (Invitrogen) were infected with FL-VP22 expressing baculovirus at a multiplicity of infection (MOI) of 3 for 48 h. FL-VP22 was purified from infected cell extract using anti-FLAG M2-agarose (Sigma), released by boiling in sample buffer and

separated from immunoglobulin chains by sodium dodecyl sulfate (SDS)–12.5% polyacrylamide gel electrophoresis. A gel strip containing FL-VP22 was isolated and used for antigen injection into rabbits (ProSci, Inc.).

A pool of monoclonal antibody to gE and a rabbit polyclonal antiserum to the cytoplasmic domain of gE have been previously described (68). Goat polyclonal antiserum to gC (serum no. 282) has been previously described (60). Mouse monoclonal antibody to GFP was purchased from Chemicon. Mouse monoclonal and rabbit polyclonal antibodies to RFP were purchased from BD Biosciences and Chemicon, respectively. Mouse monoclonal antibodies to mannosidase II (manII) and TGN38 were purchased from Covance, Inc., and Signal Transduction Laboratories, respectively.

Construction of plasmids and recombinant viruses. The plasmids EGFP-C1 (BD Biosciences), mRFP1-N1, and TD12 (17) and *Pfu* polymerase (Stratagene) were used for PCR amplification. For construction of the FLAG epitope-tagged VP22 expression vector, the UL49 open reading frame (ORF) was amplified using the forward oligonucleotide 5′-GATCTTAAGTCCAGCTCGAGAAAG AC-3′ containing an MseI site and the reverse oligonucleotide 5′-CTGAATTC AGCAAGACAGCGGACGAC-3′ containing an EcoRI site. The PCR product was digested with MseI and EcoRI and cloned into the NdeI and EcoRI sites of the FLAG fusion baculovirus transfer vector pSK277 (37) to create pTD22. For the generation of recombinant baculovirus, Sf9 cells were infected with BacPak6 (BD Biosciences) and viral DNA was isolated, digested with Bsu361, and cotransfected with pTD22 into Sf9 cells by use of Lipofectamine 2000 (Invitrogen). After complete cytopathic effect was observed, infected cells were harvested, freeze-thawed, and plated on Sf9 cells for the generation of individual plaques under an agarose overlay. Recombinant virus lacking detectable LacZ expression was plaque picked and confirmed for FL-VP22 expression by Western blotting (data not shown). For the amino-terminal fusion to UL49, the GFP ORF was amplified using the forward oligonucleotide 5′-CAGATCGATCCGCACGCGC CCGACCCCACTCGCTCGCCATGGTGAGCAAGGGCGAG-3′ containing a ClaI site and the reverse oligonucleotide 5′-TCACTCGAGCTGGACATTCCG GACTTGTACAGCTCGTC-3′ containing a XhoI site. The PCR product was digested with ClaI and XhoI and cloned into the complementary sites in pTD12, resulting in pTD27 containing a fusion of GFP to the start codon of VP22. For the carboxy-terminal fusion to UL49, the UL49 ORF was amplified using the forward oligonucleotide 5′-TCCTGGCGGTGCTCGTCGTG-3′ containing a ClaI site and the reverse oligonucleotide 5′-CATGTCGACGCTTTATACACT TTTCCCTTCCGC-3′ containing a SalI site. The PCR product was digested with ClaI and SalI and cloned into the complementary sites of pTD14 (17), resulting in pKD1 containing a fusion of the penultimate codon of UL49 to the start codon of GFP. The plasmid GS397 contains the GFP ORF inserted between codons two and three of the UL35 gene (62). The mRFP1 ORF was amplified using the forward oligonucleotide 5′-GATCCATGGCCTCCTCCGAGGACGTCATC-3′ containing the NcoI site and the reverse oligonucleotide 5′-GTATGTACACG CCGGTGGAGTGGCGGCCCTC-3′ containing a BsrG1 site and cloned into the complementary sites in pGS397. The resulting pTD55 contains a fusion of mRFP1 to the amino terminus of UL35, similar to a previously reported GFP-UL35 fusion (62).

Linearized plasmid TD27, KD1 or TD55 DNA, and PRV Becker nucleocapsid DNA were cotransfected as previously described (17) to generate PRV 178, 179, and 180, respectively. The introduction of the fluorescent fusions into the viral genome was confirmed by Southern blotting (data not shown). Virus strains encoding dual fluorescent fusion proteins were constructed by coinfection of PRV 178 or 179 with PRV 180, subsequently purified by screening dually fluorescent plaques, and confirmed by Western blotting (Fig. 1A) to generate PRV 181 and 182.

Western blot analysis. Monolayers of PK15 cells were infected with the indicated PRV strains at an MOI of 10. At 16 h postinfection, the cells were washed with phosphate-buffered saline (PBS) and harvested in radioimmunoprecipitation assay buffer (150 mM NaCl, 10 mM Tris [pH 7.4], 1% NP-40, 0.1% SDS, 0.5% sodium deoxycholate, 0.2 mM phenylmethylsulfonyl fluoride), and DNA was sheared with a needle syringe.

Virus particles were purified from the pooled medium of 12 15-cm-diameter dishes at 16 h postinfection. The medium was clarified of cell debris by centrifugation at 1,000 × *g* for 10 min at 4°C and pelleted through 30% sucrose in PBS at 100,000 × *g* (SW28 rotor) for 60 min at 4°C. The viral pellet was resuspended in TNE buffer (150 mM NaCl, 50 mM Tris [pH 7.4], 0.01 M EDTA), layered onto a 20 to 50% tartrate (dipotassium salt) linear gradient and centrifuged at 75,000 × *g* (SW41 rotor) for 16 h at 4°C. The heavy viral band was collected with a needle syringe, diluted in PAE buffer (PBS plus 2 μg of aprotinin/ml plus 1 mM EDTA, pH 8) and centrifuged at 75,000 × *g* (SW41 rotor) for 90 min at 4°C. The resulting pellet was resuspended in PAE buffer and treated by sonication. All protein samples were combined with sample buffer and separated on an SDS–12.5% polyacrylamide gel and transferred to nitrocellulose (Amersham-Pharmacia). Proteins were visualized by incubation of the nitrocellulose with primary antibodies followed by incubation with horseradish peroxidase-conjugated secondary antibodies (Kierkegaard & Perry Laboratories, Inc.) and enhanced chemiluminescence detection (Supersignal; Pierce).

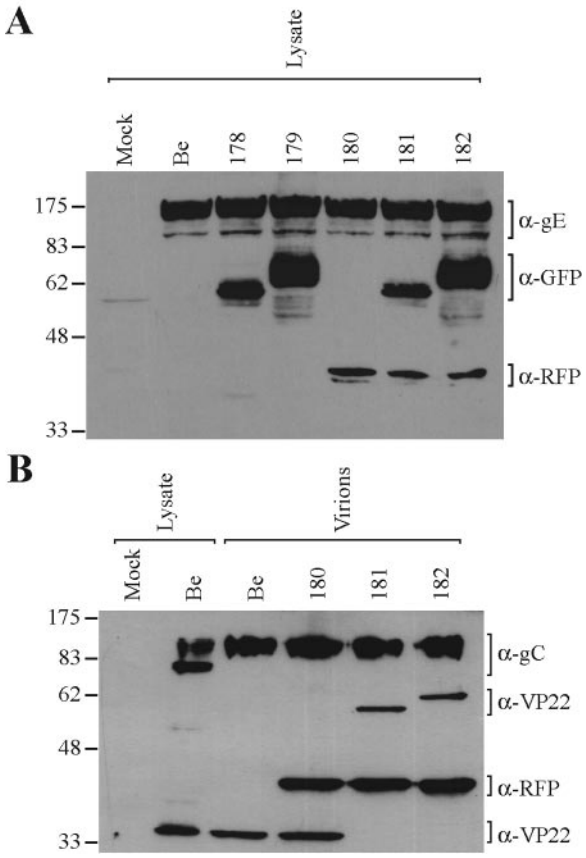

FIG. 1. Expression and virion incorporation of fluorescent fusion proteins. PK15 cells were either mock infected or infected with the indicated PRV strains at an MOI of 10 for 16 h prior to preparation of whole-cell lysates or purified extracellular virions (as indicated). Western blot analysis was performed using monoclonal antibodies to gE, GFP, and RFP (A) or polyclonal antibodies to gC, VP22, and RFP (B). The migration positions of molecular mass markers are shown on the left (in kilodaltons). Be, Becker strain.

Fluorescence-activated cell sorter (FACS) analysis. Monolayers of PK15 cells were either mock infected or infected with the indicated strains at an MOI of 10. At 6 h postinfection, cells were trypsinized briefly, washed once in PBS plus 3% bovine serum albumin (BSA), and resuspended in PBS plus 3% BSA. Ten thousand nonfixed cells were analyzed by flow cytometry (FACScan; Becton Dickinson).

Infection and BFA treatment of neurons. Dissociated SCG neurons were infected at a high MOI as previously reported (69), with the 0-h time point designated as the time of virus inoculum addition and with subsequent removal of the inoculum 1 h later. For BFA treatment, a final concentration of 1 or 2 μg of BFA (1 mg/ml stock in ethanol; Sigma)/ml was added to the medium at the indicated time. Newly prepared BFA was used since the efficacy of fungal toxin addition was found to be reduced after storage at −20°C for more than 2 weeks. For BFA recovery, the medium containing BFA was removed and cells were washed once with medium and refed with medium lacking BFA from 12 until 18 h postinfection.

Confocal microscopy of virions and live infected neurons. For direct visualization of incorporated fluorescent fusion proteins, extracellular virions were banded on a linear tartrate gradient (see above), and the heavy virion band along with a portion of the broader, light band was isolated with a needle syringe and combined with an equal volume of glycerol. A volume of 2.5 μl of virions in 50%

glycerol was spotted onto a glass slide and covered with a 22-mm^2 no. 1 coverslip (Corning), and air pockets were removed by forcibly pressing and sliding curved forceps across the coverslip to form a thin aqueous layer and then sealed with nail polish. Preparation of fluorescent virions in this manner resulted in two predominant planes of focus indicative of virion association with both glass slide and coverslip surfaces. Prepared slides were stored at −20°C prior to imaging with a 63× oil objective on a Zeiss LSM 510 microscope. Heavy particles were identified by the presence of mRFP-VP26 signal and were used to establish imaging parameters which allowed for capture of the broad range of GFP signal emitted by light and heavy particles within the linear range of detection (above background noise and below signal saturation).

Differentiated PC12 cells were infected with PRV 178 at a high MOI for approximately 12 h. Dissociated SCG neurons were infected with PRV 181 at a high MOI and treated with BFA when indicated (as described above). For the duration of live imaging, cells were maintained in RPMI medium supplemented with 25 mM HEPES (pH 7.4), 50 ng of NGF/ml, 1% horse serum, and 100 μM Trolox (Hoffmann-La Roche) (74) at 37°C under 5% CO_2 using a Delta T4 open culture system (Bioptechs) on a Zeiss LSM 510 confocal microscope.

Quantitation and analysis of fluorescent virions. The Volocity 2 software (Improvision, Inc.) was used to calculate the red and green sum emissions of PRV 181 virions. Heavy and light particles were distinguished by the colocalization of fluorescent red (capsid) and/or green (tegument) puncta (using the "measure objects" and "colocalize" functions of Volocity 2). Each fluorescent punctum identified by the software was manually confirmed and eliminated in the rare occurrence of inclusion or overlap with other puncta or debris. Particles were categorized as red alone, green alone, or green colocalized with red, and 200 extracellular virions per category were subsequently analyzed from three different virion images. A similar method was employed in the detection of fluorescent axonal puncta (beyond the initial segment) in a PRV 181-infected neuron (see Fig. 4B), with 20 puncta per category analyzed. However, the state of infection resulted in an increased background fluorescence for both red and green detection. While the green background was significantly higher than the red, both were measured, calculated as averages per axon area, and subtracted from the axonal puncta in each category.

For histogram analysis of the GFP fluorescence of PRV 181 virions, the plot starts at an emission of 5,000 arbitrary units (AU) with events placed into bins with an increasing value of 35,000 AU (see Fig. 4C). The GFP intensity values of heavy particles (see Fig. 4C) were divided by 25,954 to give a scaled histogram (see Fig. 4D). For histogram analysis of the mRFP fluorescence, events were placed into bins with an increasing value of 4,000 AU. The plotted values for mRFP fluorescence include red puncta that both do and do not colocalize with green signals above background. Unlike the fluorescence of red puncta, the detection of green puncta is partially obscured because the green signal extends into the range of background fluorescence. Since light particles that do not exhibit detectable green signals cannot be identified here, the plotted values for GFP puncta only include values above the green background, regardless of whether they colocalize with red puncta (heavy particles) or not (light particles).

Indirect immunofluorescence. Dissociated SCG neurons were infected with PRV 180 at a high MOI and treated with BFA when indicated (as described above). Infected neurons were rinsed with PBS, fixed with 3.2% paraformaldehyde for 10 min at room temperature, rinsed with PBS again, and permeabilized with PBS plus 3% BSA plus 0.1% saponin at room temperature for 10 min. Cells were then incubated with primary antisera followed by incubation with Alexa-488 goat secondary antibodies (Molecular Probes) for 30 min in PBS plus 3% BSA plus 0.1% saponin in the culture dish. Immunostaining was followed by mounting in Aqua-Poly/Mount (Polysciences, Inc.) using an 18-mm-diameter round glass coverslip (Fisher).

Ultrastructural analysis. PRV 179 virions were purified on a linear tartrate gradient (5 to 20%) as described above. The heavy virion band was collected by side puncture with a needle and used without further manipulation. Negative staining was performed by applying a 6-μl drop of virus onto Formvar-coated 300-mesh copper grids (EM Sciences) for 5 min, excess liquid was blotted away, and then a drop of 1% phosphotungstate (pH 6.3) was added for 2 min. Samples were then examined by transmission electron microscopy (see below). Dissociated SCG neurons cultured on Aclar embedding film (Electron Microscopy Sciences) were infected at a high MOI with or without treatment with 2 μg of BFA/ml at 2 h postinfection as indicated above. At the appropriate time point, infected neurons were washed twice with PBS, fixed with 2% glutaraldehyde in 0.2 M sodium cacodylate buffer (pH 7.2) for 2 to 3 h, and postfixed with 1% osmium tetroxide in sodium Veronal buffer for 1 h on ice. Samples were then rinsed with sodium Veronal buffer four times and incubated with 0.25% toluidine blue in 0.2 M cacodylate buffer (pH 7.2) for 1 h; the staining solution was then removed with four rinses of sodium Veronal buffer (pH 7.2), followed by four rinses with 0.05 M sodium maleate buffer (pH 5.1). Incubation with 2% uranyl acetate in 0.05 M sodium maleate buffer was subsequently carried out overnight in the dark followed by four rinses with 0.05 M sodium maleate buffer (pH 5.1). Fixed monolayers were then dehydrated with ethyl alcohol, embedded in Epon resin (Electron Microscopy Sciences), and cut into 70-μm-diameter sections using a Reichert Ultracut E ultramicrotome. Sections were examined using a Leo 912AB transmission electron microscope operated at 80 kV.

TABLE 1. Virus strains used in this study

PRV strain	Description
Becker	Wild type
178	GFP-VP22[a]; green fluorescent tegument
179	VP22-GFP[b]; green fluorescent tegument
180	mRFP-VP26[c]; red fluorescent capsid
181	GFP-VP22/mRFP-VP26; dual fluorescence
182	VP22-GFP/mRFP-VP26; dual fluorescence

[a] Fusion of GFP to the amino terminus of VP22.
[b] Fusion of GFP to the carboxy terminus of VP22.
[c] Fusion of mRFP1 to the carboxy terminus of VP26.

RESULTS

Transport of GFP-VP22 in the projections of living, NGF-differentiated PC12 cells. Our initial motivation was to visualize the transport of VP22, a PRV tegument component (17), in the axons of infected neurons by using fluorescent fusion proteins. In the process of constructing the appropriate viruses, we discovered some curious features of fluorescent VP22 fusion proteins that we analyzed in more detail and describe in this report. It was known that the fusion of GFP to the amino terminus of the HSV-1 VP22 homologue affected intracellular localization (23, 35). Accordingly, we constructed viral recombinants that expressed either amino- or carboxy-terminal GFP fusion proteins. PRV 178 carries a GFP fusion to the amino terminus of VP22 (GFP-VP22), while PRV 179 carries a carboxy fusion to VP22 (VP22-GFP) (Table 1). Both are predicted to carry proteins of approximately 53 kDa; however, Western blot analysis indicated that the GFP-VP22 fusion migrated as multiple bands from approximately 58 to 62 kDa (Fig. 1A). The VP22-GFP fusion exhibited an even broader signal from 62 to 78 kDa (Fig. 1A). Purified virions incorporated a 58-kDa GFP-VP22 protein and a 62-kDa VP22-GFP protein (Fig. 1B). The nature of the various forms of the VP22 fusion proteins remains to be determined.

The dissimilarity in migrating sizes of the different VP22 fluorescent fusion proteins prompted an investigation of fluorescence emission intensity of each fusion protein. We infected PK15 epithelial cells with different strains of PRV at high MOI and analyzed subsequent GFP fluorescence by FACScan. PRV Becker-infected cells developed an increase in background fluorescence relative to mock-infected cells (Fig. 2), as noted previously for PRV-infected sensory neurons (62). At 6 h postinfection, cells expressing the GFP-VP22 fusion (PRV 178) were approximately fourfold more fluorescent than cells expressing VP22-GFP (PRV 179) (Fig. 2). The distribution of fluorescence of PRV 178-infected cells was more symmetrical than that of PRV 179-infected cells. Interestingly, VP22-GFP expressed during PRV 179 infection was shown by Western blotting to have a broader migrating size (Fig. 2) and a greater heterogeneity of fluorescence than the GFP-VP22 fusion (PRV 178). Because of the more uniform fluorescence, we

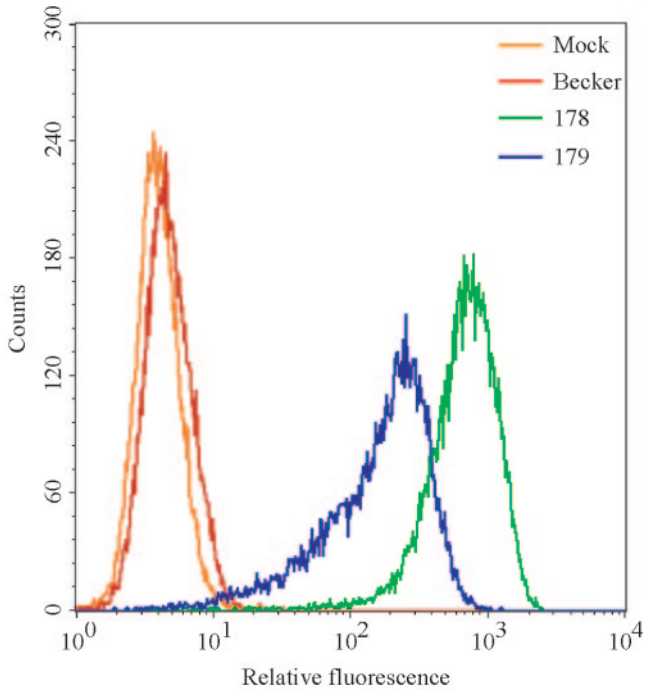

FIG. 2. Flow cytometric analysis (FACS) scatter plot. The GFP-VP22 fusion protein is brighter than the VP22-GFP fusion during infection. PK15 cells were mock infected or infected with the indicated virus strains at an MOI of 10 for 6 h and analyzed for GFP autofluorescence by FACS analysis. Infection with PRV 178 expresses GFP fused to the amino terminus of VP22 (GFP-VP22), while 179 expresses GFP fused to the carboxy terminus of VP22 (VP22-GFP).

used PRV 178 in subsequent experiments to visualize GFP-VP22 in living cells.

In our first imaging experiments, we used differentiated PC12 cells, previously shown to be susceptible and permissive for PRV infection (61). The PC12 cell line is derived from a rat adrenal pheochromocytoma, and in response to NGF, differentiates into neuronlike cells with characteristics of rat sympathetic neurons (29). This inducible cell line provides a good complement to the technically more demanding culture and infection of primary neurons. NGF-differentiated PC12 cells were infected with PRV 178 expressing GFP-VP22 for approximately 12 h. Infected cells were easily identified by the presence of GFP signals in the cell body. The axonlike projections from such cell bodies typically contained fluorescent puncta exhibiting a wide range of fluorescence intensities (Fig. 3A). When the same cultures were infected with PRV 179, we observed similar puncta, but they were less intense than those predicted from the FACS data above (data not shown).

These fluorescent puncta are capable of fast axonal transport as shown in Fig. 3B. This image represents time-lapse photography of an approximate 60-μm-wide section captured from a PC12 projection late in infection (Fig. 3A, white box). We illustrate four fluorescent puncta; one did not move (Fig. 3B, punctum 2), while three other structures, of differing fluorescent intensities, moved in the anterograde direction (away from the cell body) (Fig. 3B, left to right). Each exhibited different characteristics of movement with two moving steadily for different distances over a 15-s time period (Fig. 3B, puncta 1 and 3). These structures moved at rates of approximately 2.6 and 3.8 μm/s (puncta 1 and 3, respectively). Another punctum appeared stalled at first but then began movement at an average rate of 2.0 μm/s over 9 s, including the initial pause, before exiting the field of view (Fig. 3B, punctum 4).

The heterogeneous fluorescence of single PRV 181 particles. Despite the fluorescence heterogeneity of individual GFP-VP22 puncta, most were moving in axons at rates characteristic of fast axonal transport. One hypothesis was that the variable amounts of GFP-VP22 protein in the puncta arise from compositional differences between structures that contain a mature capsid and those that do not. We therefore tagged capsids and tegument with red and green fluorescent fusion proteins. These dual-color experiments also enabled us to determine whether capsid and tegument always moved as one unit in axons or whether they could move as separate units. We began this analysis by fusing mRFP to the amino terminus of the capsid-associated protein VP26 (mRFP-VP26), as previously described (62), to produce PRV 180. We next constructed virus strains carrying both fluorescent tegument and capsid fusion proteins by recombining PRV 178 or 179 with PRV 180; double red and green recombinants were plaque purified to produce PRV 181 and 182, respectively (Table 1). The fluorescent capsid fusion protein, mRFP-VP26, with a predicted size of 37 kDa, is observed as a 43-kDa protein in both infected cell lysates and virions (Fig. 1). Single-step growth analysis revealed that all recombinant virus strains exhibited growth similar to the parental Becker strain (data not shown). Extracellular virions purified and isolated by banding on a linear tartrate gradient (5 to 20%) were predominantly monodispersed and intact when analyzed by electron microscopy (Fig. 4A, panel a), enabling single particle analysis. The fluorescence profiles of single, extracellular PRV 181 virions were analyzed to establish imaging parameters later used for analysis of dually fluorescent puncta in axons (see Fig. 7). We were able to distinguish, by the fluorescence emissions of PRV 181 virions, infectious heavy particles (red, containing a capsid structure) from noninfectious light particles (green only, viral envelopes containing tegument, but no capsid structure). The GFP-VP22 and mRFP-VP26 fluorescence emissions of purified PRV 181 particles appeared as discrete puncta that were either exclusively red or green or a combination of the two resulting in various degrees of yellow (Fig. 4A, panel b). While the red fluorescence was uniform (approximately 42 pixels in our imaging system), the green emission was remarkably more heterogeneous. For some puncta, the radii of fluorescence of individual puncta exceeded 1 μm (Fig. 4A, panel d). Occasionally, the red and green emissions appear to be juxtaposed or only partially overlapping (Fig. 4A, panel e). PRV 182 (mRFP-VP26 and VP22-GFP) virions also exhibited heterogeneous fluorescent capsid and tegument emissions (data not shown), demonstrating that the heterogeneity of single virions is independent of the GFP fusion.

The capsid-associated protein VP26 associates with VP5 hexons in the icosahedral structure, resulting in precisely 900 copies of VP26 per individual capsid (6, 71, 76). While the precise number of mRFP-VP26 molecules incorporated into each PRV virion is presently unknown, we did expect that each capsid would contain a constant number of mRFP-VP26 molecules. Indeed, the mRFP-VP26 fluorescence profiles of indi-

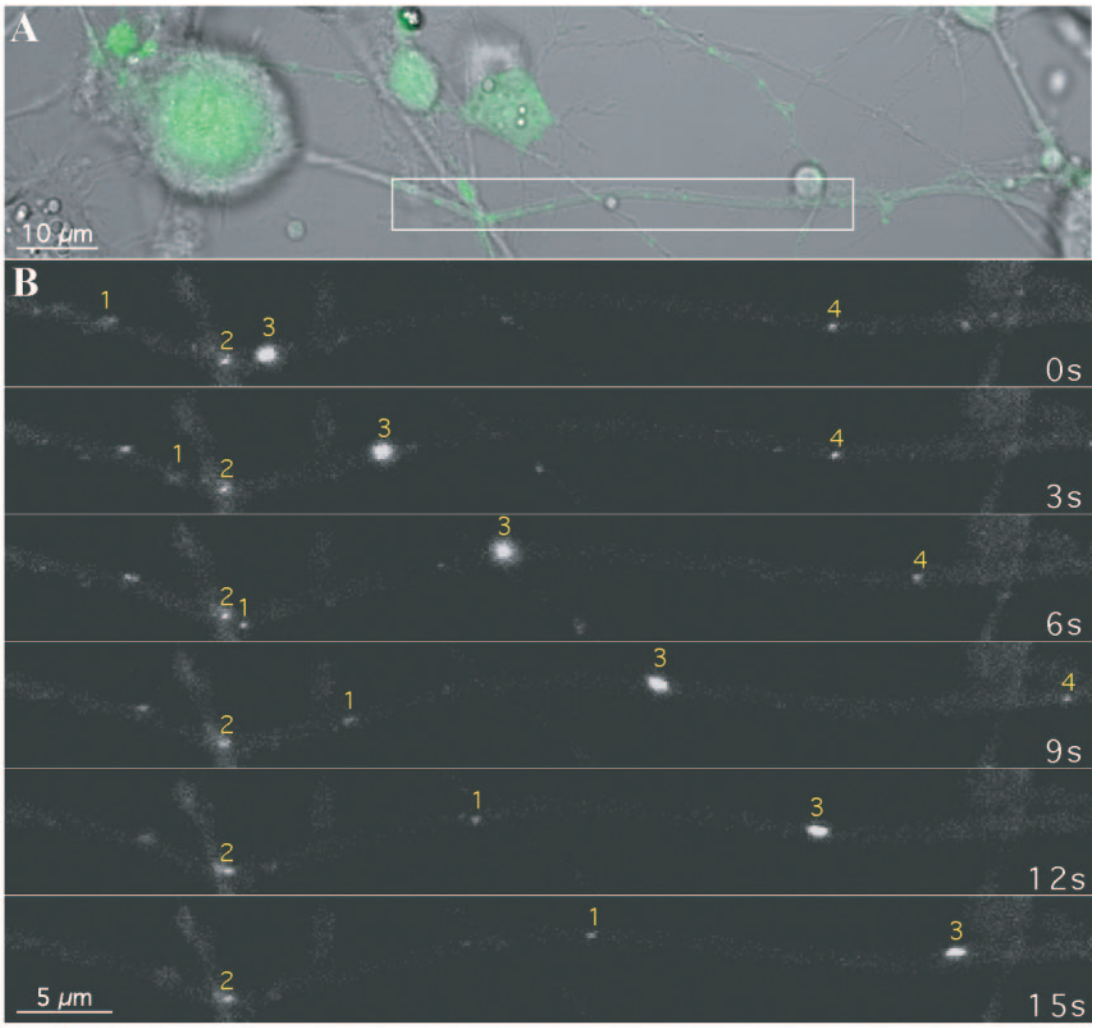

FIG. 3. Transport of GFP-VP22 structures in the axonlike projections of differentiated rat PC12 cells. PC12 cells differentiated with NGF were infected with PRV 178 at an MOI of 10 for approximately 12 h prior to live-cell confocal microscopy in a heat-controlled environment. (A) The cell bodies and projections were visualized by differential interference contrast microscopy while the GFP autofluorescence, indicative of infection, was readily detectable by confocal microscopy. (B) A section of the projection (inset in panel A) was imaged by time-lapse microscopy. Several GFP puncta of varying emission intensity are visible. The transport properties of these structures during the imaging sequence also varied; two were moving (puncta 1 and 3), one was briefly stationary and then moved (punctum 4), and another remained stationary (punctum 2).

vidual capsids approximated a Gaussian distribution consistent with this expectation (Fig. 4A, panel c). Conversely, the HSV-1 VP22 protein can be incorporated in variable amounts into virions when the protein is overexpressed (45). The presence of variable GFP emissions from GFP-VP22 in single PRV virions extends these findings and suggests that for PRV, GFP-VP22 is incorporated in variable amounts into particles even without overexpression (Fig. 4A, panel d). For a more detailed interpretation of the fluorescence profiles of single PRV 181 virions, we analyzed 200 individual heavy or light particles. Heavy particles were identified by the presence of red fluorescent puncta, while light particles were scored as emitting green fluorescence but no detectable red fluorescence (see Materials and Methods).

The quantitation of mRFP-VP26 puncta revealed a relatively symmetrical distribution of red fluorescence intensity, which was modeled by a Gaussian fit [$\chi^2_{red} = 1.47$; $df = 17$; $P(\chi^2) \cong 0.09$] (Fig. 4B). The distribution of green fluorescence from light particles exhibits a different form and is well modeled by a single decaying exponential distribution [$\chi^2_{red} = 0.966$; $df = 14$; $P(\chi^2) \cong 0.5$] (Fig. 4C, top, fit). This functional form cannot be used to describe the green fluorescence of heavy particles [fit not shown; $\chi^2_{red} = 5.8$; $P(\chi^2) < 0.001$]. Instead, these particles fall into a peaked, right-skewed distribution (Fig. 4C, bottom). This distribution resembles that expected for an intermediate in two sequential processes, but attempts to fit this functional form also failed, with a χ^2_{red} value of ~1.7 and a corresponding low probability. In addition, the mean of the green fluorescence in the light particle distribution (mean ± standard error of the mean, $1.44 \times 10^5 \pm 0.1 \times 10^5$ AU) is approximately twice that of the mean of the green fluorescence in the heavy particle distribution ($0.778 \times 10^5 \pm 0.047 \times 10^5$ AU).

The GFP-VP22 fluorescence of heavy particles appeared to

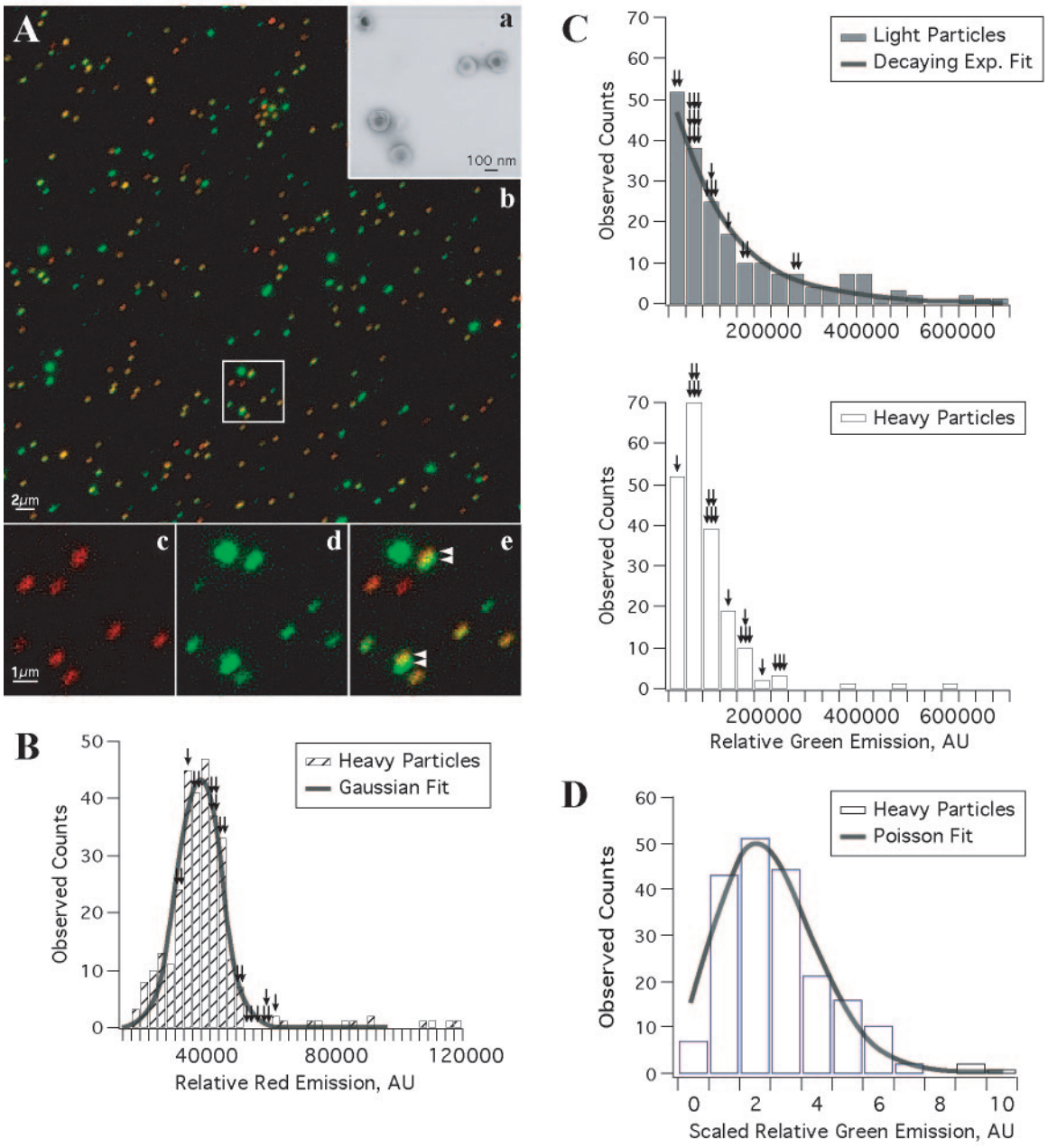

FIG. 4. Visualization and quantitation of single fluorescent virion particles. (A) (a) Extracellular virions banded on a linear tartrate gradient (5 to 20%) are predominantly intact and monodispersed as demonstrated by electron microscopy of purified PRV 179 virions. (b) The fluorescence emission of PRV 181 particles isolated by a similar method were predominantly punctate and nonoverlapping. A higher-magnification view (b, inset) illustrates the heterogeneous fluorescence emission of the virus particles: the capsid fusion (c, red) is relatively constant, while the emission of the fluorescent tegument fusion (d, green) varies considerably from particle to particle. Heavy particles from the gradient (containing capsid) were identified by red fluorescence, while light particles (lacking capsid) were identified by the presence of green and the absence of red fluorescence. (e) At times, the red and green emissions of heavy particles appear juxtaposed or only partially overlapping (arrowheads). (B to D) Histogram plot of the green and red fluorescence emissions from 200 single heavy or light particles were quantitated. (B) The red fluorescence histogram plot of heavy particles is modeled by a Gaussian curve [$\chi^2_{red} = 1.47$; $df = 17$; $P(\chi^2) \cong 0.09$]. (C) The green fluorescence histogram plot of light particles was best fit by a decaying exponential (exp.) curve [$\chi^2_{green} = 0.966$; $df = 14$; $P(\chi^2) \cong 0.5$] with a mean of $1.44 \times 10^5 \pm 0.1 \times 10^5$ AU (top, gray bars). However, the green fluorescence of heavy particles was not modeled well by this curve and exhibited a mean fluorescence of $0.778 \times 10^5 \pm 0.047 \times 10^5$ AU, approximately half that of the mean of light particle distribution (bottom, white bars). (D) Rescaling of the green fluorescence of heavy particles (shown in panel C) by a constant factor allowed for a Poisson curve fit [$\chi^2 = 5.055$; $df = 6$; $P(\chi^2) > 0.4$]. See Materials and Methods for more information on the distribution analysis. The fluorescence emissions of axonal puncta (the fluorescent equivalent of 20 heavy or light particles in axons) from the infected neuron shown in Fig. 7B are overlaid on the histograms as black arrows (with one arrow per axonal particle).

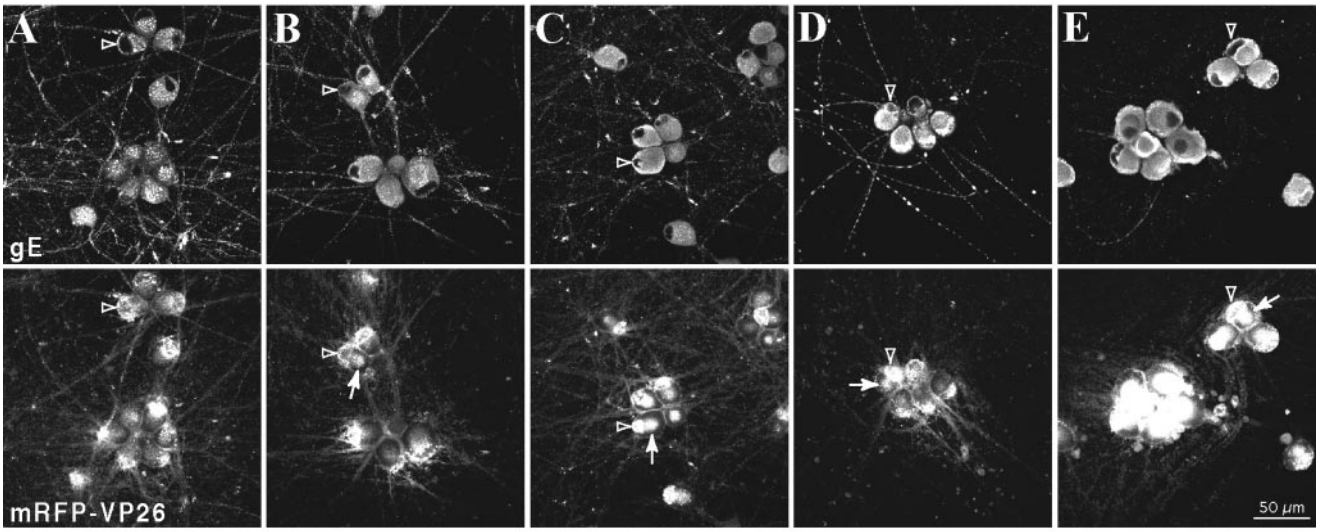

FIG. 5. Time course of BFA treatment during infection. Dissociated rat SCG neurons were infected with PRV 180 at a high MOI for 15 h prior to fixation and detection of gE localization by indirect immunofluorescence and mRFP-VP26 autofluorescence. Infected neurons were untreated (A) or subjected to a concentration of 1 μg of BFA/ml from 12 (B), 9 (C), 6 (D), or 3 (E) h postinfection until the time of fixation. Examples of nuclei of BFA-treated cells are indicated with hollow arrowheads (A to E). Cytoplasmic accumulations of fluorescent capsid are indicated with arrows (B to E).

be better described by a Poisson distribution (Fig. 4C, bottom). To test this idea, we rescaled the fluorescence intensities by a constant factor (and assumed that the magnitude of the scaling factor reflects the average size of a GFP-VP22 protein aggregation). We investigated rescaling factors such that the mean of the scaled distribution was between 1 and 5, in increments of 0.5. The best rescaling resulted in a scaled distribution with approximate equal mean and variance (mean of 2.76 and variance of 3.06) as required for a Poisson distribution (Fig. 4D, Poisson fit). Other rescalings led to larger differences between mean and variance, as well as poorer Poisson fits (as determined from χ^2). For the rescaling chosen, the Poisson fit has an (unreduced) χ^2 value of 5.055, with a value for *df* of 6, which corresponds to a value for $P(\chi^2)$ of >0.4. An interpretation of this Poisson distribution analysis is presented in Discussion.

In summary, the virion fluorescence profiles of GFP-VP22 and mRFP-VP26 were modeled by different distribution curves, with the former exhibiting broad and heterogeneous distribution and the latter exhibiting homogeneous distribution. While light particles exhibited an overall increase in GFP-VP22 fluorescence compared to heavy particles, a broad variability or heterogeneity of GFP-VP22 emissions was observed regardless of the presence or absence of a capsid structure.

Axonal entry of fluorescent capsid and tegument structures late in infection requires an intact secretory pathway. The heterogeneous puncta containing GFP-VP22 were actively moving in the projections of differentiated PC12 cells (Fig. 3B). While heavy and light extracellular particles exhibited varied GFP-VP22 composition, we still did not know whether the variable GFP-VP22 puncta observed in axonal projections were associated with capsids. Initial experiments in differentiated PC12 cells infected with the dually fluorescent PRV 181 demonstrated that GFP-VP22 puncta varied in fluorescence intensity, whether colocalized with a red mRFP signal (capsid) or not. These heterogeneous GFP-VP22 puncta also moved in the anterograde direction late in infection (data not shown). Furthermore, the distinct red, green, and yellow puncta in PRV 181-infected PC12 projections were reminiscent of the heterogeneous fluorescence of purified PRV 181 extracellular virions (data not shown). This finding raised the possibility that enveloped structures, similar to mature virions, enter axons late in infection.

We attempted to determine whether an envelopment step was necessary for the assembly and targeting of fluorescent capsid and tegument structures to the axonal compartment. We utilized BFA, a fungal toxin that blocks movement of vesicles from the endoplasmic reticulum to the *cis* Golgi compartment and is known to block herpesvirus maturation and secretion (28, 32, 46, 57, 72). In the first control experiments, we determined the effects of BFA at various times after infection in dissociated, cultured SCG neurons. We infected these primary neurons with PRV 180 (expressing mRFP-VP26) to ensure that BFA treatment did not inhibit capsid assembly in the nucleus. To determine the effects of BFA on viral envelopment, we also visualized the steady-state localization of the PRV envelope protein gE, which is predominantly localized to membranes of the endoplasmic reticulum and Golgi apparatus (67, 68). Trafficking of gE through these organelles precedes its axonal localization. Examination of the gE protein in fixed cells at 15 h postinfection by immunofluorescence revealed a reticular staining pattern throughout the cell body and abundant axonal localization in the absence of BFA treatment (Fig. 5A). A time course of treatment with 1 μg of BFA/ml added at 3, 6, 9, or 12 h postinfection disrupted gE localization in a fashion directly related to the duration of BFA exposure. While the addition of BFA at 3 h postinfection essentially prevented localization of gE to axons (Fig. 5E), when BFA was added at 6 or 9 h, entry into axons was only partially blocked (Fig. 5C and D). When BFA was added at 12 h postinfection, it was difficult to discern any effect on gE axonal localization, but a

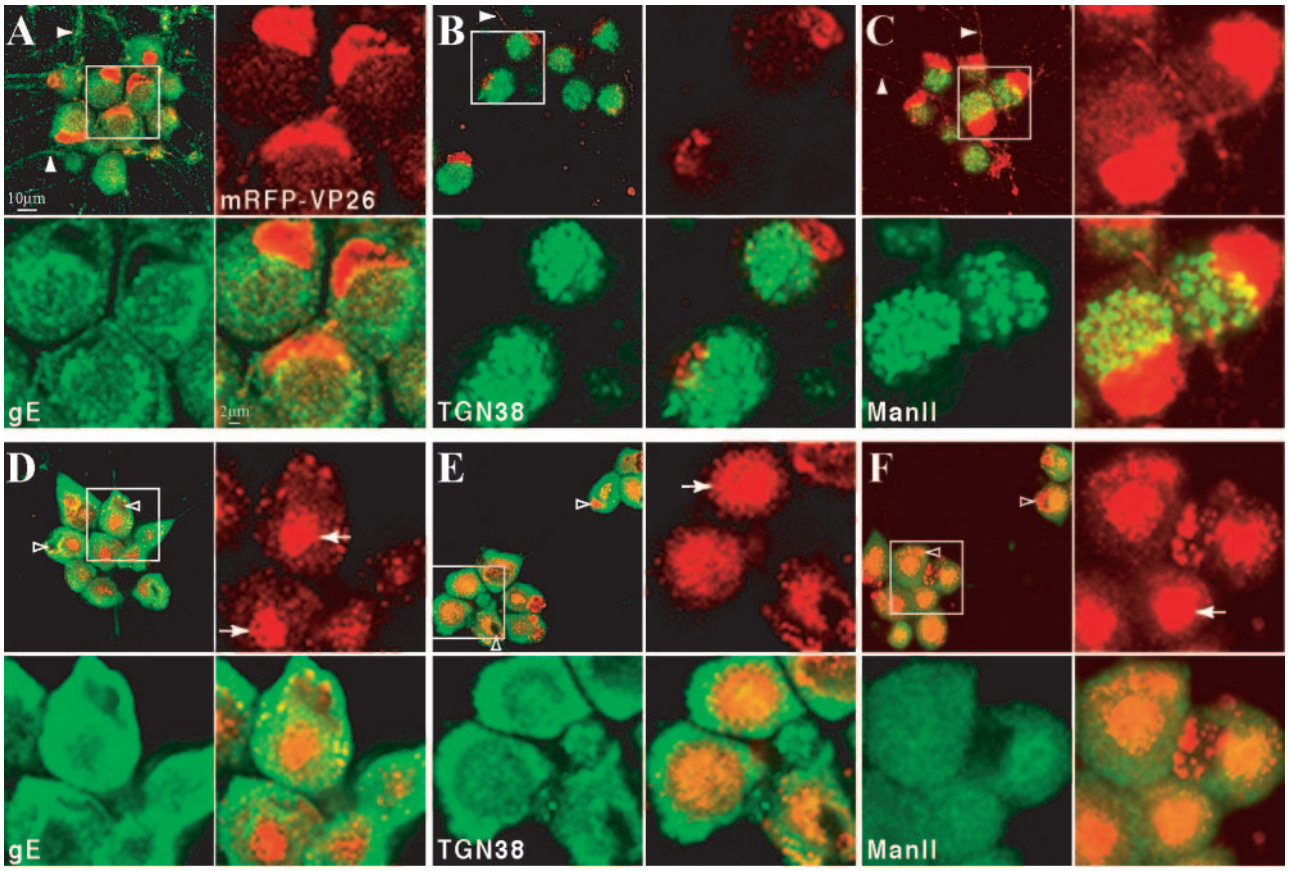

FIG. 6. Prolonged BFA treatment results in cytoplasmic accumulations of the fluorescent capsid fusion protein and disruption of the secretory pathway. Dissociated rat SCG neurons were infected with PRV 180 at a high MOI followed by incubation for 12 h (A to C) or treatment with 2 μg of BFA/ml from 2 to 12 h postinfection (D to F) prior to fixation. Autofluorescence of the mRFP-VP26 fusion (red) and indirect immunofluorescence of gE (A and D), TGN38 (B and E), or Mannosidase II (green) (C and F) is shown. Axons containing fluorescent signals are indicated with solid arrowheads (A to C), while examples of nuclei of BFA-treated cells are indicated with hollow arrowheads (D to F). Cytoplasmic accumulations of fluorescent capsid and tegument are indicated with arrows (D to F). For each sample, a region of clustered neuronal cell bodies (white box) is shown at higher magnification.

partial disruption of gE in reticular structures in the cell body was obvious (Fig. 5B). The effects of BFA on the gE steady-state localization were most evident when the fungal toxin was added at 9 h postinfection or earlier (Fig. 5C to E). We also monitored mRFP-VP26 fluorescence in these cells and found that its nuclear localization was not perturbed following BFA treatment. However, we also noted a distinctive accumulation of red fluorescence in the cytoplasm, even when BFA was added as late as 12 h postinfection (Fig. 5B). These red cytoplasmic accumulations were more intense when BFA was added at 3 h postinfection (Fig. 5E), and they varied in intensity and size when BFA was added for shorter durations. Treatment with 2 μg of BFA/ml from 2 to 12 h postinfection provided the most consistent and reproducible block in axonal targeting of gE and accumulation of mRFP-VP26 signal in the cell body (Fig. 6D to F).

The effects of treatment with 2 μg of BFA/ml on the neuronal secretory pathway were monitored by the steady-state localization of several viral and cellular markers. In non-BFA-treated neurons infected with PRV 180 (mRFP-VP26), immunostaining of gE at 12 h postinfection reveals perinuclear localization, clearly surrounding the abundant mRFP-VP26 signal in the nucleus, and a reticular staining pattern throughout the cell body (Fig. 6A). mRFP-VP26 red fluorescence is visible in axons as discrete, uniform puncta. gE is also evident in axons as distinct but more heterogeneous puncta (Fig. 6A). The ManII and TGN38 proteins are residents of the *cis*-medial Golgi and *trans* Golgi complexes, respectively (3, 8, 49). Both manII and TGN38 appear in reticular structures in the cell body during infection, but these structures do not completely surround the nucleus as observed for gE (Fig. 6B and C). Notably, manII and TGN38 invariably localize to one side of the nucleus and are not found at any detectable level in axons even late in infection (Fig. 6B and C).

BFA treatment markedly reduced the number of mRFP-VP26 fluorescent puncta in PRV 180-infected axons (Fig. 6D to F and data not shown). The localization of mRFP-VP26 in the nucleus is at times marginated and different from that observed in untreated cells (Fig. 6D to F). Accumulations of mRFP-VP26 signal in the cell body in structures near the nucleus are readily discernible (Fig. 6D to F; note that accumulations appear larger than those shown in Fig. 5 due to a larger focal plane). The reticular appearance of gE, TGN38, and manII is lost following BFA treatment and is replaced by

a perinuclear accumulation (10, 58) (Fig. 6E to F). The 6-h BFA recovery period (Fig. 7E to F) is sufficient to reverse the perinuclear distribution and partially restore the reticular localization of manII and TGN38 (data not shown).

We next assessed neurons infected with PRV 181 (GFP-VP22 and mRFP-VP26) with and without BFA treatment. Dissociated rat embryonic SCG neurons were cultured and infected with PRV 181 as described in Materials and Methods. At 12 h postinfection, live, infected neurons were imaged by confocal microscopy as described for the imaging of purified extracellular virions (Fig. 7A). Two focal planes were captured per neuron: one through the nucleus of the neuron, which lies above the plane of the axons, and the other through the axons, which lie directly on the surface of the support. The nuclei of infected cell bodies appeared yellow, indicative of colocalization of GFP-VP22 (tegument) and mRFP-VP26 (capsid) (Fig. 7A). Distinct green and red as well as yellow fluorescent patches and puncta could be seen in the cytoplasm. In the axonal plane, individual red, green, and yellow puncta were clearly observed in the cell body and initial axon segment as well as along the extent of individual axons (Fig. 7B, inset), supporting our findings for PC12 cells (data not shown). Similar localization and heterogeneity of fluorescent tegument signals were observed after PRV 182 infections (GFP-VP22/mRFP-VP26-expressing virus) (data not shown). In some instances, the punctate red and green emissions in axons appeared juxtaposed or partially overlapping as observed with purified extracellular PRV 181 particles (Fig. 7B). As infection proceeds, background green autofluorescence (not related to GFP expression [Fig. 2]) increases, which makes it difficult to discern these partially overlapping puncta.

The similarity in heterogeneity of PRV 181 extracellular virions and intra-axonal particles led us to evaluate their fluorescence by a quantitative method. We quantitated the total fluorescence emissions of 20 red puncta, green puncta alone, or green puncta colocalized with red puncta from the infected axon shown in Fig. 7B. The values for GFP emission matched those plotted for purified, extracellular PRV 181 virions (Fig. 4B and C). The axonal mRFP emission values also matched those observed for extracellular virions, with the exception of a slight shift to brighter emissions for axonal puncta relative to the extracellular peak. The shift may reflect the small sampling size or an inability to discriminate dimmer signals near the background found in infected cells.

We next determined whether BFA treatment would have a differential effect on axonal localization of GFP-VP22 and mRFP-VP26. BFA treatment had no effect on the synthesis and colocalization of fluorescent tegument and capsid protein to the nucleus during infection with PRV 181 (Fig. 7C). However, BFA treatment did induce the accumulation of colocalized fluorescent capsid and tegument protein near the nucleus (Fig. 7C). Notably, individual red, green, and yellow puncta could be seen clearly in the axonal compartment following BFA treatment, but the number of fluorescent puncta was drastically reduced (Fig. 7D). The BFA effect was reversible following the subsequent withdrawal of BFA for 6 h (Fig. 7E), in that the distribution of red and green fluorescence was similar to that observed in a non-BFA-treated sample (Fig. 7B and F).

Ultrastructural analysis of axons reveals enveloped particles late in infection. The BFA-induced accumulation of fluorescent GFP-VP22 and mRFP-VP26 signals in the cell body coincided with a severe reduction of red and green fluorescence in axons (Fig. 7B). By fluorescence, the virus structures excluded from the axonal compartment concentrated to one side of the nucleus. We investigated the ultrastructure of this BFA-induced accumulation in an attempt to gain insight into the mechanisms of virus assembly that precede axonal entry. Dissociated neurons were infected with PRV 180 as before and fixed for analysis at approximately 12 h postinfection. Enveloped particles could be observed within membrane cisternae, reminiscent of the Golgi complex, at a plane through the nucleus (Fig. 8A). These particles consist of capsid structures surrounded by a space that is not electron dense and most likely represent enveloped herpes particles, after secondary envelopment, previously reported in infected cells (11, 15, 50, 51, 72). Cytoplasmic capsids with no envelope were rare at this time postinfection (data not shown). In the electron microscope, the long-term treatment of PRV 180-infected neurons with BFA (Fig. 5 and 6) abolished membrane stacks in the cell body and revealed patches of unenveloped capsids (Fig. 7B). Notably, sections of membrane vesicles or tubes were always found among the aggregations of unenveloped capsids (Fig. 8B, inset). Nuclear arrays of capsid structures were still readily evident in the BFA-treated infected neurons (data not shown). This effect of BFA was reversible following its removal (Fig. 8C).

Numerous capsids in vesicles reminiscent of enveloped particles seen in the cell body were easily observed in sections below the nucleus, in the axonal plane. These structures were readily observed in the axon hillock and initial segment of the axonal compartment identified by organized microtubules (Fig. 9A). In contrast, following BFA treatment, vesicles and structures of this type were never seen in or near axons (Fig. 9B and data not shown). On rare occasions, unenveloped structures, possibly capsids, could be observed in BFA-treated axons (Fig. 9B).

DISCUSSION

Heterogeneity of GFP-VP22, but not mRFP-VP26, in purified light and heavy particles. Individual purified heavy and light particles of PRV 181 exhibit remarkable heterogeneity or variation in the distribution of tegument but not capsid fluorescence (Fig. 4B and C). In general, the distribution of mRFP-VP26 fluorescence in heavy virions is symmetrical and Gaussian in form, while the distribution of GFP-VP22 fluorescence is asymmetrical. Interestingly, the distribution of GFP-VP22 in heavy and light particles is not identical. The form of the different fluorescent distributions provides some insight into the mechanisms of assembly of these hybrid proteins into particles.

We assume that the amount of fluorescence emitted from a given particle reflects the amount of GFP-VP22 incorporated in that particle. The mean fluorescence of the light particle distribution (mean ± standard error of the mean, $1.44 \times 10^5 \pm 0.1 \times 10^5$ AU) was approximately twice that of the mean of the heavy particle distribution ($0.778 \times 10^5 \pm 0.047 \times 10^5$ AU). This statistically significant difference indicates that more

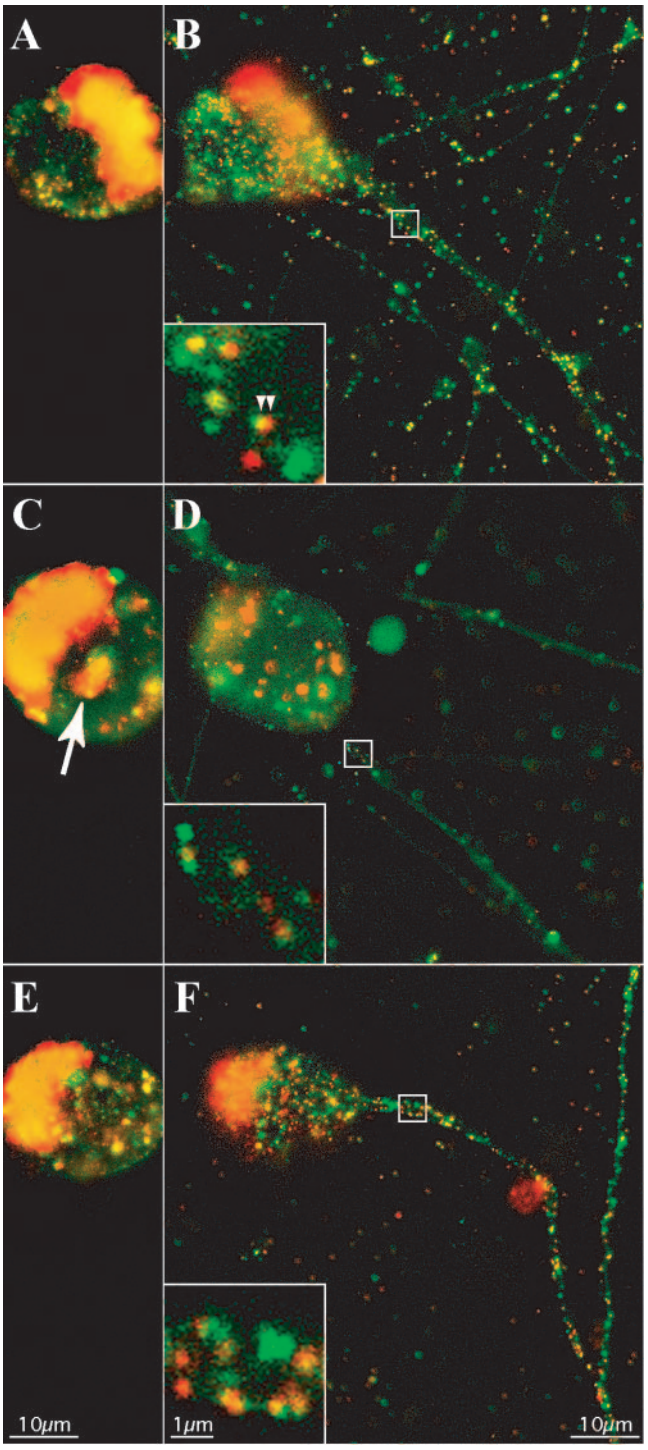

FIG. 7. Prolonged BFA treatment dramatically reduces the axonal entry of fluorescent capsid and tegument puncta. Dissociated rat SCG neurons were infected with PRV 181 at a high MOI and then subjected to incubation for 12 h (A and B), treatment with 2 μg of BFA/ml from 2 to 12 h postinfection (C and D), or treatment with BFA as before with recovery from 12 to 18 h postinfection (E and F) prior to detection of autofluorescence by confocal microscopy. Two planes of focus are shown: through the center of the nucleus, above axons (A, C, and E), or below the center of the cell body, through axons (B, D, and F). A region of axon containing fluorescent puncta (white box) is shown at a higher magnification (inset, lower left) (B, D, and F), while a cytoplasmic accumulation of fluorescent capsid and tegument is indicated with an arrow (C).

GFP-VP22 is incorporated into light particles. Second, the shapes of the distributions are different. The distribution of green fluorescence from light particles is well modeled by a single decaying exponential distribution (Fig. 4C, top). However, such a functional form cannot be used to describe the green emission of heavy particles (Fig. 4C, bottom).

Heavy-particle GFP-VP22 fluorescence was better described by a Poisson distribution, which results when a small number of independent processes contribute to the observed result. The shape of the Poisson distribution (i.e., the probability of observing one versus two versus three events) depends on the mean number of independent events. In this case, the x axis represents the measured fluorescence in arbitrary units and reflects the incorporation of many GFP-VP22 molecules. If many GFP-VP22 molecules were added independently, a Gaussian distribution would result. Instead, the observed Poisson distribution suggests that assembly of GFP-VP22 into virions involves collections of GFP-VP22 added in one step, e.g., aggregation of a "patch" of GFP-VP22 molecules on the membrane, with the entire patch attached to the capsid as a single fluorescence unit. The Poisson process reflects the number of independent patches incorporated.

To test this idea, we rescaled the fluorescence intensities by a constant factor (the magnitude reflects the average size of the GFP-VP22 protein aggregation). For the rescaling chosen, the Poisson fit has an (unreduced) χ^2 value of 5.055, with a df value of 6, which corresponds to a value for $P(\chi^2)$ of >0.4. This means that more than 40% of the time random variation alone would give such a difference, so the Poisson functional form is a reasonable model for the observed experimental data. Modeling GFP-VP22 assembly into heavy particles as a Poisson process thus suggests that on average, approximately three independent aggregates of GFP-VP22 are added to any given capsid, though as many as six could be expected (Fig. 4D). While other processes involving the capsid acting as a scaffold to direct incorporation and control the amount of VP22 added could in principle result in similar distributions, the strength of the Poisson model is that it can be tested experimentally. The model is also consistent with other studies suggesting that increased VP22 expression leads to increased incorporation of VP22 into the virion (45), as more expression would lead to more patches available for incorporation.

As noted above, the distribution of GFP-VP22 in light particles is best fit by a single decaying exponential distribution rather than a Poisson distribution. The process of GFP-VP22 assembly into light particles must therefore differ from the process producing heavy particles. One possibility is that the distribution of fluorescence reflects the size of a single GFP-VP22 aggregation. The amount of observed fluorescence reflects the size of the aggregate captured by a budding light particle. PRV 181 light particles are enriched for many small aggregates of GFP-VP22 (a large number of counts with low fluorescence [Fig. 4C, top]), a distribution largely absent in heavy particles. These data are consistent with a model in which the capsid interacts with several (about three) aggregates of GFP-VP22 and serves as a nidus of assembly, limiting the number of aggregates that assemble around the capsid. If an aggregate becomes too large, further addition will be impossible. In contrast, light particles have no capsid, so only a single aggregate can be incorporated, though the incorporated

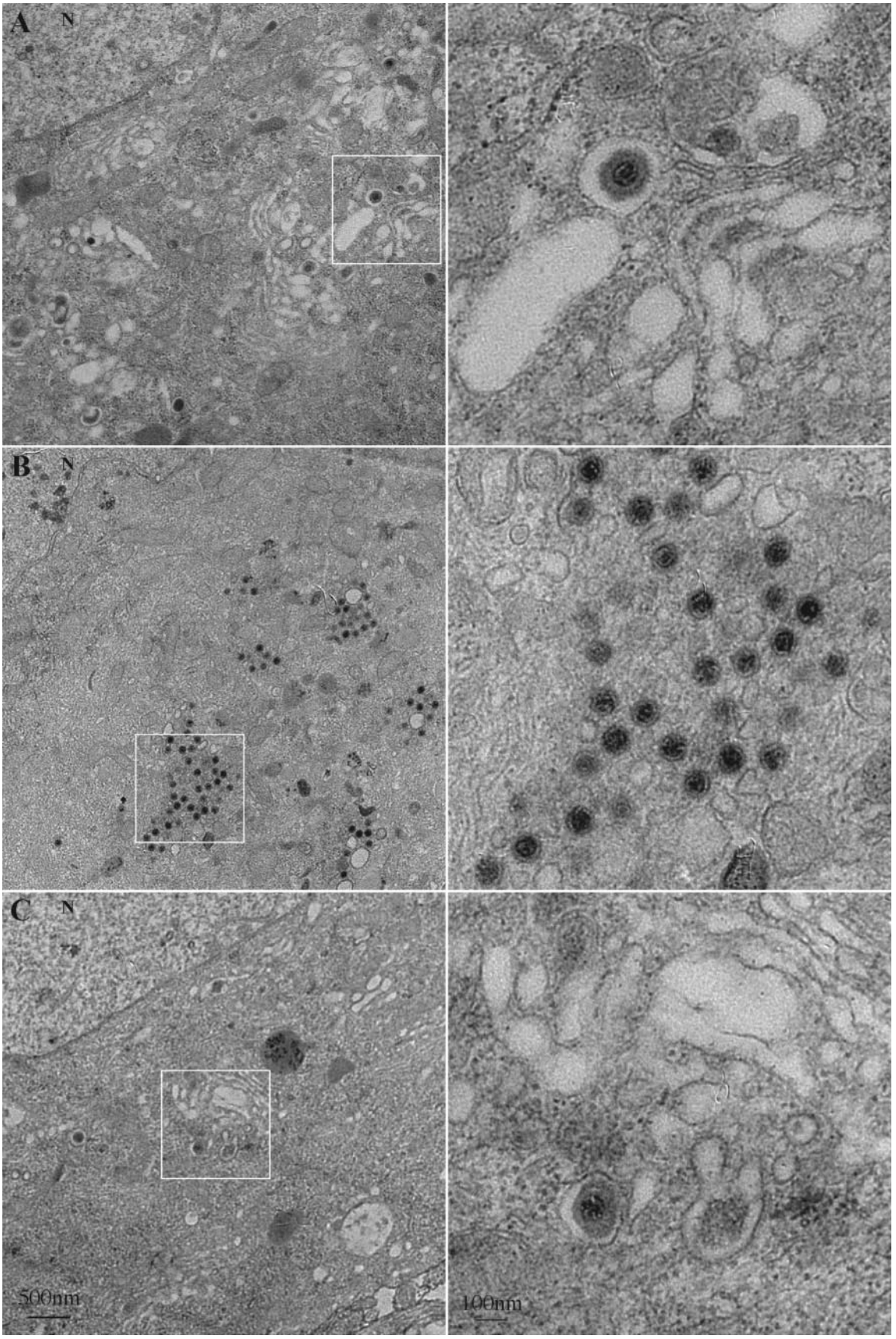

FIG. 8. Ultrastructure of the BFA-induced accumulation of virus structures in the cytoplasm of infected neurons. Dissociated rat SCG neurons were infected with PRV 180 at a high MOI followed by incubation for 12 h (A), treatment with 2 μg of BFA/ml from 2 to 12 h postinfection (B) or treatment with BFA as before with recovery from 12 to 18 h postinfection (C) prior to fixation and processing for transmission electron microscopy. For each sample, a region of the neuronal cell body (left, white box) is shown at a higher magnification (right). N indicates the nucleus.

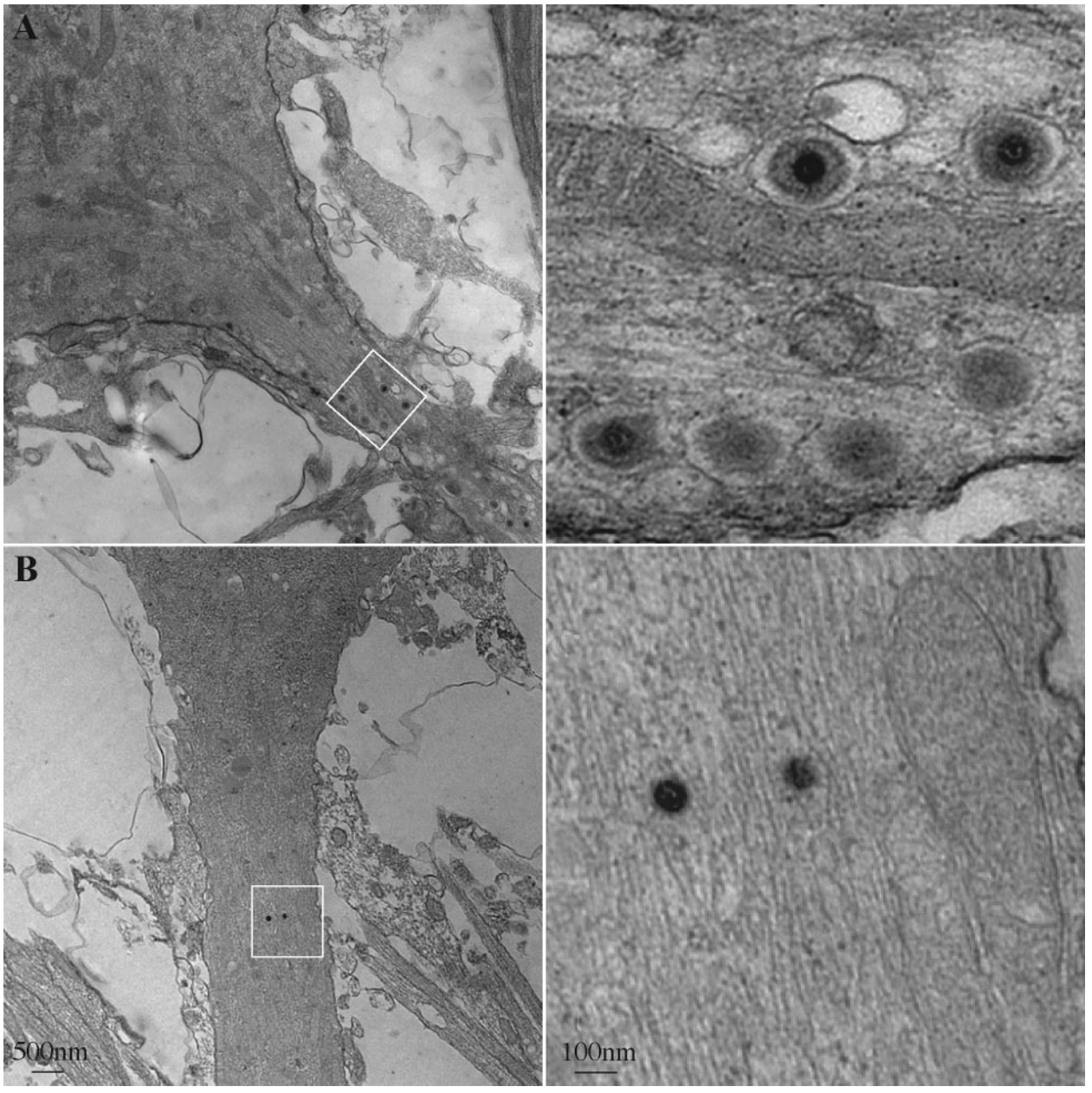

FIG. 9. Enveloped virus particles are restricted from axons following the BFA treatment of infected neurons. Dissociated rat SCG neurons were infected with PRV 180 at a high MOI followed by incubation for 12 h (A) or treatment with 2 μg of BFA/ml from 2 to 12 h postinfection (B) prior to fixation and processing for transmission electron microscopy. A proximal region (A) or more distal region (B) of the axonal projection (left, white box) is shown at a higher magnification (right).

aggregate can be of a larger size than those added to capsids. Our analyses suggest a dynamic interplay between assemblies of GFP-VP22 and the capsid in which the capsid influences the incorporation of GFP-VP22 in functional aggregates of moderate size. The absence of these interactions in light particle formation may account for the observably different incorporation of GFP-VP22.

As a control of our experimental protocols, we examined the mRFP-VP26 fluorescence emitted by PRV 181 virions. Previously, the fluorescence plot of a GFP-VP26 fusion protein in purified nucleocapsids resembled a Gaussian distribution (62). The mRFP-VP26 distribution in purified heavy particles was also Gaussian [$\chi^2_{red} = 1.47$; $df = 17$; $P(\chi^2) \cong 0.09$] (Fig. 4B). This finding suggests that either fusion protein (GFP-VP22 or mRFP-VP26) is incorporated within a narrow range of copy number per single virion structure and is consistent with its incorporation into the regular-shaped, icosahedral capsid structure.

The heterogeneity in virus particles containing both a fluorescent capsid and a tegument fusion protein is noteworthy and provides some insight into mechanisms of particle assembly. Occasionally we observed fluorescent tegument puncta juxta-

posed to fluorescent capsid puncta in the axonal compartment, reminiscent of the asymmetrical tegument described by Grunewald et al. (Fig. 7B, inset). However, we cannot rule out the close apposition of two separate red and green fluorescent structures. While the fluorescence of the capsid fusion (mRFP-VP26) was fairly homogeneous, that of the tegument fusion (GFP-VP22) was heterogeneous (Fig. 4). This heterogeneity is not restricted to the GFP-VP22 PRV recombinants. Preliminary data showed that the fluorescence of a GFP fusion to the viral gM incorporated in single virus particles was more heterogeneous than that of the capsid fusion (data not shown). Further work is necessary to extend these studies, but by using combinations of fluorescently tagged virion proteins, it should be possible to determine the extent of heterogeneity in single-particle protein composition.

Axonal entry and transport of fluorescent capsid and tegument structures following replication. Using time-lapse microscopy, we demonstrated that the heterogeneous GFP-VP22 structures observed in axons were actively transported in differentiated PC12 cells. These differentiated cells are similar to primary sympathetic neuron cultures (29). GFP-VP22 puncta of different fluorescent intensities moved in saltatory runs at rates similar to those previously reported for the fast axonal anterograde transport of viral structures (34, 62). In the present experiment, it was not possible to determine whether these moving puncta were associated with capsid structures. PRV 181, a recombinant strain that expresses both GFP-VP22 and mRFP-VP26, provided a tool to make this determination. Both GFP-VP22 and mRFP-VP26 localize to the cytoplasmic and axonal compartments of cultured primary infected neurons by 12 h postinfection (Fig. 7B). However, the GFP-VP22 puncta in axons often were distinct and not associated with the mRFP-VP26 signal (Fig. 7B). In addition, mRFP-VP26 puncta were found in axons with and without the association of detectable amounts of the GFP-VP22 fusion. It is likely that tegument structures containing undetectable amounts of GFP-VP22 also enter the axons of infected neurons. At present, we have not determined the limits of detection of GFP-VP22 by confocal microscopy. Similar to purified virions, puncta of the red fluorescent capsid fusion protein (mRFP-VP26) in axons were uniform in fluorescence (Fig. 4 and 7), while the GFP-VP22 signal in axons was far more heterogeneous (Fig. 3B and 7). We have preliminary time-lapse data demonstrating that both mRFP-VP26 and GFP-VP22 structures move in axons separately and together, seemingly independent of the intensity of GFP-VP22 (data not shown).

Given that the heterogeneity observed in mature virions must arise during the process of assembly, it may be that similar structures are also moved into axons for long-distance transport. Indeed, the fluorescence of individual puncta in axons exhibits a distribution similar to that of purified extracellular virions (Fig. 4). An important question concerns the composition of structures destined for axons. They may be assembly intermediates preceding secondary envelopment or mature virions. Some evidence supports the hypothesis that partially assembled virion components, rather than mature or fully assembled virions, enter and move along the axonal compartment. These virion subassemblies comprise collections of mature viral glycoproteins separated from the capsid structure (34, 44, 53, 56, 69). Consistent with this hypothesis, the treatment of infected neurons with the secretory pathway inhibitor, BFA, did not inhibit entry of HSV-1 capsid antigen into the axonal compartment during infection (53). An important consideration comes from studies of nonneuronal cells. Here, the final stages of virion assembly involves a tightly coupled interaction of capsids, select tegument proteins, and mature membrane proteins in the process of secondary envelopment (reviewed in reference 52). How these highly interactive events could be uncoupled in neurons prior to targeting to the axonal compartment remains an open question.

In rat SCG neurons infected with PRV 181, the addition of BFA at 2 h postinfection, a time prior to viral late gene expression, had little effect on viral protein synthesis in the cell body but severely reduced axonal entry of fluorescent capsid and tegument puncta, regardless of whether they were together or separate (Fig. 7D). The BFA block was not complete, and a small fraction of capsid and tegument structures were still visible in axons. At present, we are unable to say whether these remaining structures originate from entry or egress events during infection. Our observation that BFA treatment blocks axonal entry of PRV capsid structures contrasts with previous reports for HSV-1 (53, 54). In our hands, a short 3-h treatment resulted in a detectable accumulation of fluorescent capsid signal in the cell body (Fig. 5B). Given the high degree of gene conservation between HSV-1 and PRV (52), it seems likely that both alphaherpesviruses would utilize similar mechanisms for axonal entry and transport. Therefore, the difference may reflect the experimental conditions. One idea is that axonal entry of glycoproteins and tegument can be blocked by concentrations of BFA that are not sufficient to inhibit entry of capsid structures. Another possibility is that HSV-1 infections of the human dorsal root ganglion cultures and the PRV infections of rat SCG neuron display differential sensitivity to BFA (14, 53).

Our BFA analysis implicates the secretory pathway in the axonal entry of both capsid and tegument structures. BFA treatment results in the relocalization of TGN38 to immunoreactive vesicles throughout the neuronal cytoplasm (48). We observed a similar disruption of the reticular localization of TGN38 following BFA treatment (Fig. 6E) as well as an accumulation of vesicles around capsids in the cytoplasm of treated, infected neurons (Fig. 8B). It may be that interactions between tegument-capsid structures and Golgi membranes are maintained despite the disruption of Golgi membrane stacks by BFA treatment. It will be important to identify the cellular components of these BFA-induced vesicles. We were concerned that the use of long-term BFA treatment may affect cell viability and therefore indirectly disrupt axonal transport of viral proteins. However, we eliminated the concern of irreversible effects by demonstrating that the phenotype of BFA-treated neurons is reversible (Fig. 7E and F). Importantly, data from electron microscopy revealed an abundance of enveloped capsids in axons (Fig. 9A) and a lack of enveloped capsids in axons following BFA treatment (Fig. 9B). Taken together, our data demonstrate that the majority of capsid, and possibly tegument, structures enter the axon late in infection within the lumen of a vesicle. This suggests that the absence of this membrane during capsid entry, and its presence during egress, provides the preferential interaction with different classes of motors that regulates directional transport in axons. However,

since our BFA treatment does not completely prevent the axonal localization of fluorescent capsid and tegument puncta, a small population of unenveloped particles may still enter axons under these conditions (Fig. 7B). Furthermore, our ultrastructure analysis does not include all planes and sections of infected neurons and may not be sensitive enough to resolve the axonal entry of a small percentage of unenveloped capsids. We have also noted an absence of colocalization with the synaptic vesicle markers SV2 and VAMP2 (data not shown). Therefore, although our data support a model in which many capsid and tegument structures enter axons in vesicles late in infection, we cannot exclude the possibility that a population of unenveloped capsid and tegument structures also enters the axon compartment.

Indirect immunofluorescence studies and direct fluorescence of fusion proteins have demonstrated a marked heterogeneity of virus assemblies, including a partial colocalization of capsid structures with viral membrane proteins and select tegument proteins (62, 69; our unpublished observations). It is difficult to reconcile such observations with a model in which mature virions in transport vesicles are moved solely in axons. We speculate that more viral proteins enter axons than are found in assembling virions. For example, viral membrane proteins are found in the axonal plasma membrane (our unpublished observations and Ch'ng and Enquist, unpublished). This finding suggests that select viral components can enter axons independent of virion maturation. Accordingly, it is difficult with the imaging technology used in this report to distinguish virion components that enter as assembly intermediates from those that enter as independent units (not in virus assemblies). We must still entertain two possibilities: a subpopulation of assembled capsid structures may enter axons within a Golgi complex-derived vesicle lacking integral viral proteins, while viral membrane proteins and membrane-associated tegument proteins enter axons independently. Alternatively, a subpopulation of capsids and tegument might reside in mature virions transported in vesicles. PRV VP22 is reported to interact with the viral glycoproteins E and M (27). It would be interesting to know whether GFP-VP22 is always associated with gE and gM in axons. At present, it is unknown whether tegument structures not associated with capsids enter the axonal compartment within a membrane vesicle. Similarly, it is not known whether light particles (viral membrane proteins and tegument but no capsid) enter axons, although we often observed bright GFP-VP22 puncta with no detectable red mRFP-VP26 signal in axons. The origin and constituents of the membrane surrounding capsids shown by ultrastructure analysis (Fig. 9A) are under investigation.

The heterogeneity of fluorescent virus particles. As we have discussed, the heterogeneity of GFP-VP22 in virus particles provides some insight into mechanisms of particle assembly. Approximately 33 different virus-borne structural proteins comprise the mature PRV particle, with about 12 previously demonstrated to reside in the envelope and another 12 in the tegument layer (36). If our findings with fluorescent fusion proteins reflect assembly events for wild-type virions, it may be that no two mature virus particles are identical in composition. The biological significance of such heterogeneity remains to be determined. Perhaps this variability provides more opportunities for escape from innate and immune defenses. In addition, one subpopulation of virus particles may have a propensity for the productive infection of one cell type or organism versus another. As the heterogeneity of fluorescent tegument fusion proteins was also observed in axons late in infection, it may also be that no two virus assemblies in axons are identical. The effects of this putative heterogeneity on transneuronal spread of PRV in the nervous system remains to be explained. Finally, single-virus-particle imaging requires that proteins be altered with fluorescent tags. A caveat in these analyses, therefore, is that we are unable to visualize the wild-type proteins. Nevertheless, imaging technology provides new insights into the general problem of virion assembly and transmission of infection.

ACKNOWLEDGMENTS

We acknowledge Roger Tsien for providing pmRFP1-N1, Greg Smith for pGS397, and Richard Young for pSK277, without which this work would not have been possible. Princeton University staff members Joe Goodhouse and Margaret Bisher provided expert assistance in confocal and electron microscopy, while Christina DeCoste performed expert FACS services. Thanks to Kathy M. Daumer for constructing pKD1 and PRV 179.

This work was supported by NIH grant 2ROI-NS33506 to L. W. Enquist and an NIH Research Supplement for Underrepresented Minority to T. del Rio. S. P. Gross is supported by NIH-ROI grant GM-64624-01.

REFERENCES

1. **Baines, J. D., R. J. Jacob, L. Simmerman, and B. Roizman.** 1995. The herpes simplex virus 1 UL11 proteins are associated with cytoplasmic and nuclear membranes and with nuclear bodies of infected cells. J. Virol. **69:**825–833.
2. **Banfield, B. W., J. D. Kaufman, J. A. Randall, and G. E. Pickard.** 2003. Development of pseudorabies virus strains expressing red fluorescent proteins: new tools for multisynaptic labeling applications. J. Virol. **77:**10106–10112.
3. **Baron, M. D., and H. Garoff.** 1990. Mannosidase II and the 135-kDa Golgi-specific antigen recognized monoclonal antibody 53FC3 are the same dimeric protein. J. Biol. Chem. **265:**19928–19931.
4. **Bearer, E. L., X. O. Breakefield, D. Schuback, T. S. Reese, and J. H. LaVail.** 2000. Retrograde axonal transport of herpes simplex virus: evidence for a single mechanism and a role for tegument. Proc. Natl. Acad. Sci. USA **97:**8146–8150.
5. **Bestvater, F., T. A. Knoch, J. Langowski, and E. Spiess.** 2002. Construct conversions caused by simultaneous co-transfection: "GFP-walking." BioTechniques **32:**844–850.
6. **Booy, F. P., B. L. Trus, W. W. Newcomb, J. C. Brown, J. F. Conway, and A. C. Steven.** 1994. Finding a needle in a haystack: detection of a small protein (the 12-kDa VP26) in a large complex (the 200-MDa capsid of herpes simplex virus). Proc. Natl. Acad. Sci. USA **91:**5652–5656.
7. **Brignati, M. J., J. S. Loomis, J. W. Wills, and R. J. Courtney.** 2003. Membrane association of VP22, a herpes simplex virus type 1 tegument protein. J. Virol. **77:**4888–4898.
8. **Burke, B., G. Griffiths, H. Reggio, D. Louvard, and G. Warren.** 1982. A monoclonal antibody against a 135-K Golgi membrane protein. EMBO J. **1:**1621–1628.
9. **Campbell, R. E., O. Tour, A. E. Palmer, P. A. Steinbach, G. S. Baird, D. A. Zacharias, and R. Y. Tsien.** 2002. A monomeric red fluorescent protein. Proc. Natl. Acad. Sci. USA **99:**7877–7882.
10. **Campenot, R. B., J. Soin, M. Blacker, K. Lund, H. Eng, and B. L. MacInnis.** 2003. Block of slow axonal transport and axonal growth by brefeldin A in compartmented cultures of rat sympathetic neurons. Neuropharmacology **44:**1107–1117.
11. **Card, J. P., L. Rinaman, R. B. Lynn, B. H. Lee, R. P. Meade, R. R. Miselis, and L. W. Enquist.** 1993. Pseudorabies virus infection of the rat central nervous system: ultrastructural characterization of viral replication, transport, and pathogenesis. J. Neurosci. **13:**2515–2539.
12. **Chatterjee, S., and S. Sarkar.** 1992. Studies on endoplasmic reticulum-Golgi complex cycling pathway in herpes simplex virus-infected and brefeldin A-treated human fibroblast cells. Virology **191:**327–337.
13. **Cheung, P., B. W. Banfield, and F. Tufaro.** 1991. Brefeldin A arrests the maturation and egress of herpes simplex virus particles during infection. J. Virol. **65:**1893–1904.
14. **Ch'ng, T. H., A. E. Flood, and L. W. Enquist.** 2004. Culturing primary and transformed neuronal cells for studying pseudorabies virus infection. Methods Mol. Biol. **292:**299–316.

15. **Cook, M. L., and J. G. Stevens.** 1973. Pathogenesis of herpetic neuritis and ganglionitis in mice: evidence for intra-axonal transport of infection. Infect. Immun. **7:**272–288.
16. **Dasgupta, A., and D. W. Wilson.** 2001. Evaluation of the primary effect of brefeldin A treatment upon herpes simplex virus assembly. J. Gen. Virol. **82:**1561–1567.
17. **del Rio, T., H. C. Werner, and L. W. Enquist.** 2002. The pseudorabies virus VP22 homologue (UL49) is dispensable for virus growth in vitro and has no effect on virulence and neuronal spread in rodents. J. Virol. **76:**774–782.
18. **Desai, P., and S. Person.** 1998. Incorporation of the green fluorescent protein into the herpes simplex virus type 1 capsid. J. Virol. **72:**7563–7568.
19. **DiCicco-Bloom, E., W. J. Friedman, and I. B. Black.** 1993. NT-3 stimulates sympathetic neuroblast proliferation by promoting precursor survival. Neuron **11:**1101–1111.
20. **Diefenbach, R. J., M. Miranda-Saksena, E. Diefenbach, D. J. Holland, R. A. Boadle, P. J. Armati, and A. L. Cunningham.** 2002. Herpes simplex virus tegument protein US11 interacts with conventional kinesin heavy chain. J. Virol. **76:**3282–3291.
21. **Donnelly, M., and G. Elliott.** 2001. Nuclear localization and shuttling of herpes simplex virus tegument protein VP13/14. J. Virol. **75:**2566–2574.
22. **Donnelly, M., and G. Elliott.** 2001. Fluorescent tagging of herpes simplex virus tegument protein VP13/14 in virus infection. J. Virol. **75:**2575–2583.
23. **Elliott, G., and P. O'Hare.** 1999. Live-cell analysis of a green fluorescent protein-tagged herpes simplex virus infection. J. Virol. **73:**4110–4119.
24. **Enquist, L. W.** 2002. Exploiting circuit-specific spread of pseudorabies virus in the central nervous system: insights to pathogenesis and circuit tracers. J. Infect. Dis. **186**(Suppl. 2)**:**S209–S214.
25. **Everett, R. D., G. Sourvinos, and A. Orr.** 2003. Recruitment of herpes simplex virus type 1 transcriptional regulatory protein ICP4 into foci juxtaposed to ND10 in live, infected cells. J. Virol. **77:**3680–3689.
26. **Field, H. J., and T. J. Hill.** 1974. The pathogenesis of pseudorabies in mice following peripheral inoculation. J. Gen. Virol. **23:**145–157.
27. **Fuchs, W., B. G. Klupp, H. Granzow, C. Hengartner, A. Brack, A. Mundt, L. W. Enquist, and T. C. Mettenleiter.** 2002. Physical interaction between envelope glycoproteins E and M of pseudorabies virus and the major tegument protein UL49. J. Virol. **76:**8208–8217.
28. **Fujiwara, T., K. Oda, S. Yokota, A. Takatsuki, and Y. Ikehara.** 1988. Brefeldin A causes disassembly of the Golgi complex and accumulation of secretory proteins in the endoplasmic reticulum. J. Biol. Chem. **263:**18545–18552.
29. **Greene, L. A., and A. S. Tischler.** 1976. Establishment of a noradrenergic clonal line of rat adrenal pheochromocytoma cells which respond to nerve growth factor. Proc. Natl. Acad. Sci. USA **73:**2424–2428.
30. **Greene, L. A., D. E. Burstein, and M. M. Black.** 1982. The role of transcription-dependent priming in nerve growth factor promoted neurite outgrowth. Dev. Biol. **91:**305–316.
31. **Grunewald, K., P. Desai, D. C. Winkler, J. B. Heymann, D. M. Belnap, W. Baumeister, and A. C. Steven.** 2003. Three-dimensional structure of herpes simplex virus from cryo-electron tomography. Science **302:**1396–1398.
32. **Helms, J. B., and J. E. Rothman.** 1992. Inhibition by brefeldin A of a Golgi membrane enzyme that catalyses exchange of guanine nucleotide bound to ARF. Nature **360:**352–354.
33. **Hill, T. J., H. J. Field, and A. P. Roome.** 1972. Intra-axonal location of herpes simplex virus particles. J. Gen. Virol. **15:**233–235.
34. **Holland, D. J., M. Miranda-Saksena, R. A. Boadle, P. Armati, and A. L. Cunningham.** 1999. Anterograde transport of herpes simplex virus proteins in axons of peripheral human fetal neurons: an immunoelectron microscopy study. J. Virol. **73:**8503–8511.
35. **Hutchinson, I., A. Whiteley, H. Browne, and G. Elliott.** 2002. Sequential localization of two herpes simplex virus tegument proteins to punctate nuclear dots adjacent to ICP0 domains. J. Virol. **76:**10365–10373.
36. **Klupp, B. G., C. J. Hengartner, T. C. Mettenleiter, and L. W. Enquist.** 2004. Complete, annotated sequence of the pseudorabies virus genome. J. Virol. **78:**424–440.
37. **Koh, S. S., C. J. Hengartner, and R. A. Young.** 1997. Baculoviral transfer vectors for expression of FLAG fusion proteins in insect cells. BioTechniques **23:**622–626–627.
38. **Kopp, M., H. Granzow, W. Fuchs, B. G. Klupp, E. Mundt, A. Karger, and T. C. Mettenleiter.** 2003. The pseudorabies virus UL11 protein is a virion component involved in secondary envelopment in the cytoplasm. J. Virol. **77:**5339–5351.
39. **Koyama, A. H., and T. Uchida.** 1994. Inhibition by Brefeldin A of the envelopment of nucleocapsids in herpes simplex virus type 1-infected Vero cells. Arch. Virol. **135:**305–317.
40. **Kristensson, K., B. Ghetti, and H. M. Wisniewski.** 1974. Study on the propagation of Herpes simplex virus (type 2) into the brain after intraocular injection. Brain Res. **69:**189–201.
41. **Kristensson, K., E. Lycke, M. Roytta, B. Svennerholm, and A. Vahlne.** 1986. Neuritic transport of herpes simplex virus in rat sensory neurons in vitro. Effects of substances interacting with microtubular function and axonal flow [nocodazole, taxol and erythro-9-3-(2-hydroxynonyl)adenine]. J. Gen. Virol. **67:**2023–2028.
42. **La Boissiere, S., A. Izeta, S. Malcomber, and P. O'Hare.** 2004. Compartmentalization of VP16 in cells infected with recombinant herpes simplex virus expressing VP16-green fluorescent protein fusion proteins. J. Virol. **78:**8002–8014.
43. **LaVail, J. H., K. S. Topp, P. A. Giblin, and J. A. Garner.** 1997. Factors that contribute to the transneuronal spread of herpes simplex virus. J. Neurosci. Res. **49:**485–496.
44. **LaVail, J. H., A. N. Tauscher, E. Aghaian, O. Harrabi, and S. S. Sidhu.** 2003. Axonal transport and sorting of herpes simplex virus components in a mature mouse visual system. J. Virol. **77:**6117–6126.
45. **Leslie, J., F. J. Rixon, and J. McLauchlan.** 1996. Overexpression of the herpes simplex virus type 1 tegument protein VP22 increases its incorporation into virus particles. Virology **220:**60–68.
46. **Lippincott-Schwartz, J., L. C. Yuan, J. S. Bonifacino, and R. D. Klausner.** 1989. Rapid redistribution of Golgi proteins into the ER in cells treated with brefeldin A: evidence for membrane cycling from Golgi to ER. Cell **56:**801–813.
47. **Lippincott-Schwartz, J., J. G. Donaldson, A. Schweizer, E. G. Berger, H. P. Hauri, L. C. Yuan, and R. D. Klausner.** 1990. Microtubule-dependent retrograde transport of proteins into the ER in the presence of brefeldin A suggests an ER recycling pathway. Cell **60:**821–836.
48. **Lowenstein, P. R., E. E. Morrison, D. Bain, A. F. Shering, G. Banting, P. Douglas, and M. G. Castro.** 1994. Polarized distribution of the trans-Golgi network marker TGN38 during the in vitro development of neocortical neurons: effects of nocodazole and brefeldin A. Eur. J. Neurosci. **6:**1453–1465.
49. **Luzio, J. P., B. Brake, G. Banting, K. E. Howell, P. Braghetta, and K. K. Stanley.** 1990. Identification, sequencing and expression of an integral membrane protein of the trans-Golgi network (TGN38). Biochem. J. **270:**97–102.
50. **Lycke, E., K. Kristensson, B. Svennerholm, A. Vahlne, and R. Ziegler.** 1984. Uptake and transport of herpes simplex virus in neurites of rat dorsal root ganglia cells in culture. J. Gen. Virol. **65:**55–64.
51. **Lycke, E., B. Hamark, M. Johansson, A. Krotochwil, J. Lycke, and B. Svennerholm.** 1988. Herpes simplex virus infection of the human sensory neuron. An electron microscopy study. Arch. Virol. **101:**87–104.
52. **Mettenleiter, T. C.** 2000. Aujeszky's disease (pseudorabies) virus: the virus and molecular pathogenesis—state of the art, June 1999. Vet. Res. **31:**99–115.
53. **Miranda-Saksena, M., P. Armati, R. A. Boadle, D. J. Holland, and A. L. Cunningham.** 2000. Anterograde transport of herpes simplex virus type 1 in cultured, dissociated human and rat dorsal root ganglion neurons. J. Virol. **74:**1827–1839.
54. **Miranda-Saksena, M., R. A. Boadle, P. Armati, and A. L. Cunningham.** 2002. In rat dorsal root ganglion neurons, herpes simplex virus type 1 tegument forms in the cytoplasm of the cell body. J. Virol. **76:**9934–9951.
55. **Openshaw, H., and W. G. Ellis.** 1983. Herpes simplex virus infection of motor neurons: hypoglossal model. Infect. Immun. **42:**409–413.
56. **Penfold, M. E., P. Armati, and A. L. Cunningham.** 1994. Axonal transport of herpes simplex virions to epidermal cells: evidence for a specialized mode of virus transport and assembly. Proc. Natl. Acad. Sci. USA **91:**6529–6533.
57. **Randazzo, P. A., Y. C. Yang, C. Rulka, and R. A. Kahn.** 1993. Activation of ADP-ribosylation factor by Golgi membranes. Evidence for a brefeldin A- and protease-sensitive activating factor on Golgi membranes. J. Biol. Chem. **268:**9555–9563.
58. **Reaves, B., and G. Banting.** 1992. Perturbation of the morphology of the trans-Golgi network following Brefeldin A treatment: redistribution of a TGN-specific integral membrane protein, TGN38. J. Cell Biol. **116:**85–94.
59. **Roizman, B., and E. Sears.** 1996. Herpes simplex viruses and their replication, p. 1043–1107. *In* B. N. Fields, D. M. Knipe, and P. M. Howley (ed.), Fundamental virology. Lippincott-Raven, Philadelphia, Pa.
60. **Ryan, J. P., M. E. Whealy, A. K. Robbins, and L. W. Enquist.** 1987. Analysis of pseudorabies virus glycoprotein gIII localization and modification by using novel infectious viral mutants carrying unique EcoRI sites. J. Virol. **61:**2962–2972.
61. **Schilter, B., and C. M. Marchand.** 1991. Effects of pseudorabies virus on the neuronal properties of PC12 cells. J. Neurochem. **56:**898–906.
62. **Smith, G. A., S. P. Gross, and L. W. Enquist.** 2001. Herpesviruses use bidirectional fast-axonal transport to spread in sensory neurons. Proc. Natl. Acad. Sci. USA **98:**3466–3470.
63. **Smith, G. A., L. Pomeranz, S. P. Gross, and L. W. Enquist.** 2004. Local modulation of plus-end transport targets herpesvirus entry and egress in sensory axons. Proc. Natl. Acad. Sci. USA **101:**16034–16039.
64. **Sodeik, B., M. W. Ebersold, and A. Helenius.** 1997. Microtubule-mediated transport of incoming herpes simplex virus 1 capsids to the nucleus. J. Cell Biol. **136:**1007–1021.
65. **Sourvinos, G., and R. D. Everett.** 2002. Visualization of parental HSV-1 genomes and replication compartments in association with ND10 in live infected cells. EMBO J. **21:**4989–4997.
66. **Tamura, G., K. Ando, S. Suzuki, A. Takatsuki, and K. Arima.** 1968. Antiviral activity of brefeldin A and verrucarin A. J. Antibiot. (Tokyo) **21:**160–161.
67. **Tirabassi, R. S., R. A. Townley, M. G. Eldridge, and L. W. Enquist.** 1997. Characterization of pseudorabies virus mutants expressing carboxy-terminal

truncations of gE: evidence for envelope incorporation, virulence, and neurotropism domains. J. Virol. **71:**6455–6464.
68. **Tirabassi, R. S., and L. W. Enquist.** 2000. Role of the pseudorabies virus gI cytoplasmic domain in neuroinvasion, virulence, and posttranslational N-linked glycosylation. J. Virol. **74:**3505–3516.
69. **Tomishima, M. J., and L. W. Enquist.** 2001. A conserved alpha-herpesvirus protein necessary for axonal localization of viral membrane proteins. J. Cell Biol. **154:**741–752.
70. **Topp, K. S., L. B. Meade, and J. H. LaVail.** 1994. Microtubule polarity in the peripheral processes of trigeminal ganglion cells: relevance for the retrograde transport of herpes simplex virus. J. Neurosci. **14:**318–325.
71. **Trus, B. L., F. L. Homa, F. P. Booy, W. W. Newcomb, D. R. Thomsen, N. Cheng, J. C. Brown, and A. C. Steven.** 1995. Herpes simplex virus capsids assembled in insect cells infected with recombinant baculoviruses: structural authenticity and localization of VP26. J. Virol. **69:**7362–7366.
72. **Whealy, M. E., J. P. Card, R. P. Meade, A. K. Robbins, and L. W. Enquist.** 1991. Effect of brefeldin A on alphaherpesvirus membrane protein glycosylation and virus egress. J. Virol. **65:**1066–1081.
73. **Willard, M.** 2002. Rapid directional translocations in virus replication. J. Virol. **76:**5220–5232.
74. **Wu, T. W., N. Hashimoto, J. Wu, D. Carey, R. K. Li, D. A. Mickle, and R. D. Weisel.** 1990. The cytoprotective effect of Trolox demonstrated with three types of human cells. Biochem. Cell Biol. **68:**1189–1194.
75. **Yamamoto, T., S. Otani, and H. Shiraki.** 1973. Ultrastructure of herpes simplex virus infection of the nervous system of mice. Acta Neuropathol. **26:**285–299.
76. **Zhou, Z. H., J. He, J. Jakana, J. D. Tatman, F. J. Rixon, and W. Chiu.** 1995. Assembly of VP26 in herpes simplex virus-1 inferred from structures of wild-type and recombinant capsids. Nat. Struct. Biol. **2:**1026–1030.